

NOTE TO USERS

This reproduction is the best copy available.

UMI[®]

OFDM Systems: Symbol Error Rate Evaluation, Filter Bank Design and Joint Maximum Likelihood Detection

by

YUHONG WANG

(MEng, Beijing University of Aeronautics and Astronautics, China, 1995)

(BSc, Beijing University of Aeronautics and Astronautics, China, 1992)

A thesis

presented to Ryerson University

in partial fulfillment of the

requirement for the degree of

Master of Applied Science

in the Program of

Electrical and Computer Engineering

Toronto, Ontario, Canada, 2003

©YUHONG WANG 2003

UMI Number: EC52901

INFORMATION TO USERS

The quality of this reproduction is dependent upon the quality of the copy submitted. Broken or indistinct print, colored or poor quality illustrations and photographs, print bleed-through, substandard margins, and improper alignment can adversely affect reproduction.

In the unlikely event that the author did not send a complete manuscript and there are missing pages, these will be noted. Also, if unauthorized copyright material had to be removed, a note will indicate the deletion.

UMI[®]

UMI Microform EC52901

Copyright 2009 by ProQuest LLC.

All rights reserved. This microform edition is protected against unauthorized copying under Title 17, United States Code.

ProQuest LLC
789 E. Eisenhower Parkway
PO Box 1346
Ann Arbor, MI 48106-1346

Abstract

OFDM Systems: Symbol Error Rate Evaluation, Filter Bank Design and Joint
Maximum Likelihood Detection

YUHONG WANG

Master of Applied Science of Electrical and Computer Engineering
Ryerson Universtiy

A closed-form symbol error rate (SER) formula for a generic OFDM system with M -ary phase shift keying (MPSK) modulation, and optimal phase detector for each subchannel, is derived. By employing the derived SER formula as the objective function, a novel OFDM system based on designed complex-valued unitary filter banks is presented to minimize the SER. A detection algorithm is presented for a generic OFDM system to *jointly* detect subchannel symbols received in one time frame. Monte-Carlo numerical simulations are performed to verify the theoretical SER analysis and compare the error performance of the proposed OFDM system with DFT-based OFDM and DWMT systems, and the new joint detection algorithm with the conventional subchannel detection algorithm. The above efforts provide systematic approaches for the OFDM error performance analysis and the OFDM system design.

Keywords: OFDM system, MPSK, symbol error rate, unitary filter bank, joint maximum likelihood detection.

Acknowledgment

I appreciate the support and encouragement from Dr. Xiao-Ping Zhang, my supervisor. His expertise in communications and filter banks is very helpful for this work.

I would like to thank all the committee members for their participation in my thesis defense.

I would like to thank the Electrical and Computer Engineering department at Ryerson University for the financial support of my study and research.

I would like to thank all staff of the Electrical and Computer Engineering at Ryerson University for their kind help.

I wish to convey the warmest thanks to my family for their endless support.

Contents

1	Introduction	1
2	Principles of Digital Filter Banks	6
2.1	Fundamentals of Digital Filter Bank	7
2.1.1	Basic Building Blocks	8
2.1.2	Polyphase Structures	10
2.1.3	Perfect Reconstruction Property	13
2.2	Filter Bank Based Transmultiplexer	14
2.2.1	TDM and FDM	14
2.2.2	Perfect Reconstruction Transmultiplexer	16
2.3	Summary	18
3	Orthogonal Frequency Division Multiplexing (OFDM) Systems	19
3.1	Basic Principles of OFDM	20
3.1.1	Data Generation and Modulation	20
3.1.2	OFDM Transmultiplexer	22
3.2	DFT-Based OFDM and DWMT	24
3.2.1	DFT-based OFDM	24
3.2.2	Discrete Wavelet Multitone Systems	27
3.3	Summary	29
4	Symbol Error Rate Evaluation and Filter Bank Design for OFDM Systems with MPSK Modulation	30

4.1	Symbol Error Rate Evaluation for OFDM Systems with MPSK Modulation	32
4.1.1	System Modelling	32
4.1.2	Symbol Error Rate for Generic MPSK-OFDM Systems	33
4.1.3	SER Expression for AWGN Channels	40
4.1.4	SER Expression for Fading Channels	41
4.2	Complex-Valued Unitary Filter Bank Based OFDM System Design	42
4.2.1	Parameterization of Filter Bank Coefficients	43
4.2.2	SER Improvement Based on Proposed Filter Banks	44
4.3	Simulations	45
4.4	Summary	51
5	Joint Maximum Likelihood Detection Algorithm for OFDM Systems and Error Performance Analysis	54
5.1	Joint Detection Algorithm for OFDM Systems	56
5.1.1	System Modelling	56
5.1.2	Constellation Points of Received Vector Symbols	57
5.1.3	Joint Detection of Received Vector Symbol	62
5.1.4	Error Performance Analysis	64
5.1.5	Discussions	67
5.2	Simulations	67
5.3	Summary	69
6	Conclusions and Future Research	72
6.1	Conclusions	72
6.2	Future Research	74
A	Central Limit Theorem	75
B	Change of Variables	77

List of Figures

2.1	Block diagram of a generic digital filter bank	7
2.2	Ideal magnitude responses in a P -subchannel filter bank	8
2.3	Demonstration of decimation for $K = 2$	8
2.4	Demonstration of the interpolator for $K = 2$	9
2.5	Noble identities of multirate systems	11
2.6	The polyphase representation of a P -band maximally decimated filter bank	12
2.7	The simplification of polyphase representation of P -band maximally decimated filter bank	13
2.8	(a) Time domain multiplexing (b) Time domain demultiplexing.	14
2.9	The operation of a frequency division multiplexer.	15
2.10	The transmultiplexer based on filter bank structure	16
2.11	(a) Equivalent structures for the transmultiplexer using polyphase matrices, (b) rearrangement using noble identities, (c) simplified structure.	17
3.1	The block diagram for an OFDM transceiver	20
3.2	Data parsing function in an OFDM transceiver. The number of subchannels $P = 3$. Sign ‘.’ represents single binary symbol	21
3.3	The block diagram of an OFDM transmultiplexer	22
3.4	The construction of output of transmitting filters	23
3.5	Subchannel frequency responses of DFT-based OFDM system for $\omega \in [0, 0.88]$ and $P = 32$	26

3.6	The stylized plot of CP inclusion. The l_k long CP can also be the trailing zeroes.	27
3.7	The schematic diagram of a DFT-based OFDM system	27
3.8	Frequency responses of a DWMT system for $\omega \in [0, 0.88]$ and $P = 32$	29
4.1	Block diagram for filter bank modulator and demodulator in OFDM systems	32
4.2	Error performance of single carrier modulation and the conventional DWMT ($g = 2$) modulation with BPSK	41
4.3	Error performance of the conventional DWMT systems ($g = 2$) over channel $c(n) = [1, 0.5e^{j\pi/6}, 0.3e^{-j\pi/3}, 0.2e^{j\pi/2}, 0.1]$	42
4.4	Flowchart of system simulation	47
4.5	Comparison of the analytical and simulated performance of OFDM systems over AWGN channels: QPSK ($P = 16$)	48
4.6	Comparison of the analytical and simulated performance of OFDM systems over AWGN channels: QPSK ($P = 32$)	48
4.7	Amplitude characteristics of frequency responses of two channels used in simulations	49
4.8	Comparison of the analytical and simulated performance of OFDM systems with QPSK coding over channel $c_1(n)$ ($P = 16$)	50
4.9	Comparison of the analytical and simulated performance of OFDM systems with QPSK coding over channel $c_2(n)$ ($P = 16$).	50
4.10	Comparison of the analytical and simulated performance of OFDM systems with QPSK coding over channel $c_1(n)$ ($P = 32$)	51
4.11	Comparison of the analytical and simulated performance of OFDM systems with QPSK coding over channel $c_2(n)$ ($P = 32$).	51
4.12	System performance of different OFDM systems with QPSK modulation over channel $c_1(n)$ ($P = 32$).	52
4.13	System performance of different OFDM systems with QPSK modulation over channel $c_2(n)$ ($P = 32$).	52

5.1	Block diagram for filter bank modulator and demodulator in OFDM systems	56
5.2	Schematic illustration of ML detector	64
5.3	Calculation of SER under joint detection algorithm	69
5.4	Comparison of joint detection and subchannel detection over an AWGN channel with BPSK ($P = 32$)	70
5.5	Comparison of joint detection and subchannel detection over channel $c_1(n)$ with BPSK ($P = 32$)	70
5.6	Comparison of joint detection and subchannel detection over channel $c_2(n)$ with BPSK ($P = 32$)	71
B.1	Illustration of change of variables	77

Chapter 1

Introduction

IN recent years, multi-carrier modulation (MCM) has become increasingly popular as a transmission technique, especially in high speed communications, including wireline and wireless systems. The principle of MCM consists of splitting up a wideband signal at a high symbol rate into several lower rate signals, each one occupying a narrower band, so called a subchannel or a subcarrier. By dividing the input data stream into parallel substreams, and each stream being modulated and multiplexed onto one of subchannels at different carrier frequencies, the power spectrum of the transmitted signal can be shaped to match the channel characteristics to achieve near optimal performance theoretically. The general recognized advantage of the MCM is its robustness against different types of channel distortions, such as multipath propagation and narrowband interferences [1, 2, 3].

Orthogonal frequency division multiplexing (OFDM), as the most important class of the MCM, has been under intensive research and development in recent years [4, 5, 6, 7]. In the OFDM modulation, subcarriers are made mutually orthogonal so that the receiver can separate these subcarriers even there is spectral overlapping among them. The MCM approach adopted in OFDM is the filtered multitone, in which a filter bank modulator and demodulator transfers time-division multiplexed (TDM) data to frequency-division multiplexed (FDM) data and vice versa [8, 9]. A filter bank modulator divides the spectra of communication channels into a set of spectrally overlapping or non-overlapping subchannels, and the aliasing caused by spectral overlapping will be removed by a fil-

ter bank demodulator, if the filter bank modulator and demodulator fulfills the perfect reconstruction (PR) property [10].

Mainly two types of filter banks have been adopted as modulators and demodulators in OFDM systems. The application of the first one, discrete Fourier transform (DFT) filter banks, was proposed decades ago [11] and has found broad applications such as very high-speed digital subscriber lines (VDSL) [12], European digital audio broadcasting (DAB), European digital video broadcasting (DVB) and short-range wireless access and wireless LAN standards (IEEE802.11a). A DFT filter bank exhibits the desired mutual orthogonality of subchannels and can be implemented with a fast Fourier transform (FFT) algorithm. The other type of the filter banks, which are generated from a well designed prototype filter via extended lapped transform (ELT), have been proposed for discrete wavelet multitone (DWT) systems as another realization of the OFDM modulation [13, 14, 15]. Adopted as one of signaling standards for asymmetric digital subscriber lines (ADSL), a DWT system can achieve a high level of subchannel spectral containment so that it is more robust with regard to interchannel interference and narrow band channel noise compared to the DFT-based OFDM system [13, 16].

In most practical OFDM systems, the mutual orthogonality of subchannels is often destroyed by non-ideal transmission channels. The transmitted symbols for a given subchannel may be distorted by co-subchannel symbols (intersymbol interference or ISI) and symbols on the other subchannels (interchannel interference or ICI), as well as the channel noise. For the DFT-based OFDM system, the high degree of spectral overlaps among the subchannels of DFT filter banks makes it difficult to retain subchannel isolation for multipath channels, therefore a technique in which a 'cyclic prefix' is inserted at the beginning of each data segment has been adopted, at the cost of system efficiency [2, 8], to partially offset the interference introduced by communication channels. Due to the existence of ISI, ICI and channel noise in an OFDM system, the precise error performance evaluation can not be readily obtained. Recently some attempts based on certain assumptions and bounds have been made to investigate the error performance of the OFDM systems

[6, 17, 18, 19, 20, 21]. The absence in these efforts includes the following two topics:

- a. The error performance evaluation has been conducted only for the DFT-based OFDM systems. However, the error performance of a *generic* OFDM system, in which the modulation filters form a set of orthonormal basis, and the filter bank modulator and demodulator fulfill the PR property, such as the DWMT systems, has not been systematically investigated.
- b. The detection algorithm adopted for OFDM systems has been the conventional subchannel detection algorithm, under which the detection and decoding is done per received subchannel symbol by considering effects from all the other symbols, except the one to be decoded, as interference. Consequently, under this detection algorithm, for a given subchannel, information carried by the symbols of the other subchannels is not used for obtaining a better evaluation of symbols transmitted on the given subchannel and to improve the system error performance.

Both of the above topics are addressed in this thesis. The error performance of a generic OFDM system, with DFT-based OFDM and DWMT as two realizations, is studied by considering the effects of both interference and additive channel Gaussian noise. By studying the constellations of received symbols and the interference for a given subchannel, and modelling the sum of ISI and ICI as a Gaussian process using the Central Limit Theorem, the statistical probability of the received symbol on a given subchannel is investigated. Furthermore, a closed-form expression of the symbol error rate (SER) is derived for a generic OFDM system employing MPSK modulation and the conventional optimal phase detector in each subchannel. This SER formula can be applied to both the DFT-based OFDM and the DWMT systems. It can also be used as a design criterion for an OFDM system. This SER formula is verified with numerical Monte-Carlo simulations by employing DFT based OFDM systems and conventional discrete wavelet multitone (DWMT) systems. Simulation results are consistent with the derived formula. This work is presented in [22].

In addition, by using the derived SER formula as the objective function, a novel OFDM system based on designed complex-valued unitary filter banks with improved system error performance is presented. A unitary filter bank is a good candidate to OFDM modulator/demodulator due to the inherent mutual orthogonality between filters. In addition, unlike to real-valued coefficient filters, complex-valued filters have asymmetric frequency responses and are more suitable to deal with complex-valued signals which are often present in wireless systems. Filters in the presented OFDM system are parameterized with free parameters, which can be adjusted to various applications. In this thesis, the free parameters are determined to minimize the SER by employing the derived SER as the objective function. Simulation results show that the designed OFDM system outperforms the conventional DWMT systems in terms of SER and has comparable SER performance with the DFT-based OFDM systems [22]. By taking different objective functions, the complex-valued filter banks can be adjusted to various criterions in OFDM design as presented in [23, 24].

To address the topic *b*, a detection algorithm for a generic OFDM system which jointly detects and decodes subchannel symbols received in one frame, is presented. The main advantage of this joint detection algorithm is that, it turns the mutual effects of jointly decoded subchannel symbols, from interference to useful information contributing to the constellation points of each other. The received symbols from a subset of subchannels are considered as the multidimensional vector symbols and the constellation points of the vector symbols are derived. Based on derived constellation points, maximum likelihood (ML) criterion is employed in detecting the vector symbol. Lower and upper bounds of the vector symbol error rate is presented. Simulations are conducted to compare the detection performance under the proposed joint detection algorithm and the conventional subchannel detection algorithm. It is shown that the joint detection algorithm outperforms the subchannel detection algorithm for both DFT-based OFDM and DWMT systems. This part of work is presented in [25].

Outline: The remainder of this thesis is organized as follows. In Chapter 2, the

fundamentals of digital filter banks, which act as the modulator and demodulator for the OFDM transmission, are introduced. In Chapter 3, the basic principles and properties of an OFDM system are summarized. In Chapter 4, a closed-formed SER formula is derived, for a generic OFDM system with MPSK modulation and the optimal phase detector for each subchannel. A novel OFDM system, based on designed complex-valued unitary filter banks, is presented. In Chapter 5, a new joint detection algorithm and error performance analysis under this algorithm are introduced. Chapter 6 concludes the thesis and proposes several topics for further work.

Notations: Boldface lower-case letters are used to represent vectors, and boldface upper-case letters are reserved for matrices. The notations \mathbf{A}^T and \mathbf{A}^H represent the transpose and transpose-conjugate (Hermitian) of \mathbf{A} , respectively. The superscript ' $*$ ', \mathbf{A}^* , denotes the conjugation only. The Kronecker function $\delta(n)$ is defined as

$$\delta(n) = \begin{cases} 1, & n = 0, \\ 0, & n \neq 0. \end{cases} \quad (1.1)$$

The notation $\text{diag}(a_0, a_1, \dots, a_{P-1})$ denotes an $P \times P$ diagonal matrix with diagonal elements a_k , $k = 0, 1, \dots, P - 1$.

Chapter 2

Principles of Digital Filter Banks

THE idea of subdividing a signal frequency band into a set of subbands was recognized very early in the fields of multirate signal processing, where subband partitioning was introduced to perform short-time spectrum analysis of speech signals, initially in analog and then in digital form. It was later found that, for the digital representation of speech signals, if the subbands are individually quantized (subband coding) with possibly different accuracy, it is possible to achieve, for the same total bit rate, a signal quality better than that obtained by quantizing the full-band signal. Over the last two decades, this discipline of technology has found applications in image compression, the digital audio industry, statistical and adaptive signal processing and in many other fields [26, 27]. It also fits naturally with certain special classes of time-frequency representations such as the short-time Fourier transform and the wavelet transform, which are useful in analyzing the time-varying nature of signal spectra.

The principal element for the spectral splitting is the perfect reconstruction (PR) quadrature mirror filter (QMF) bank. The PR QMF structure allows spectral decomposition into a set of overlapping segments in such a way that the aliasing incurred in the initial ‘analysis stage’ is eliminated during signal reconstruction by the ‘synthesis’ stage, and all the amplitude and phase distortion is completely eliminated in the reconstructed signal.

In this chapter, the fundamentals of digital filter banks, with emphasis on maximally

decimated QMF filter banks, are presented. The topics to be discussed include operations of decimation and interpolation in Section 2.1.1, polyphase structures in Section 2.1.2 and the property of PR in Section 2.1.3. In addition, the filter bank based transmultiplexer, which acts as the modulator and demodulator in MCM systems, is introduced in Section 2.2. Section 2.3 summarizes this chapter.

This chapter provides a summary of the principles of digital filter banks as presented in [10, 26, 28].

2.1 Fundamentals of Digital Filter Bank

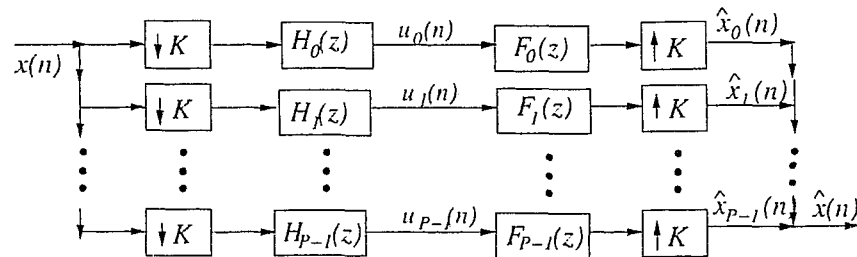


Figure 2.1: Block diagram of a generic digital filter bank

Fig. 2.1 illustrates a generic form of a QMF digital filter bank with P subbands. The upsampling / downsampling factor is denoted as K and $K \leq P$. As shown in Fig. 2.1, a filter bank can be a parallel arrangement of a set of filters with a common input (analysis filter bank) or with the output of the filters summed to generate a single synthesized signal (synthesis filter bank). The analysis filter bank, $\{h_0(n), h_1(n), \dots, h_p(n)\}$, with $h_p(n)$ denoted as the impulse response for the p th-filter for $0 \leq p \leq P-1$, splits the signal $x(n)$ into P subband signals. In frequency domain, the analysis filter bank splits the spectrum of $x(n)$ into P uncorrelated subbands. Fig. 2.2 shows the ideal magnitude responses in a P subband filter bank. The synthesis bank $\{f_0(n), f_1(n), \dots, f_{P-1}(n)\}$, combines P signals $\{\hat{x}_0(n), \hat{x}_1(n), \dots, \hat{x}_{P-1}(n)\}$ into one signal $\hat{x}(n)$, typically called the reconstructed signal.

A filter bank is said to be critically sampled or maximally decimated when $K = P$.

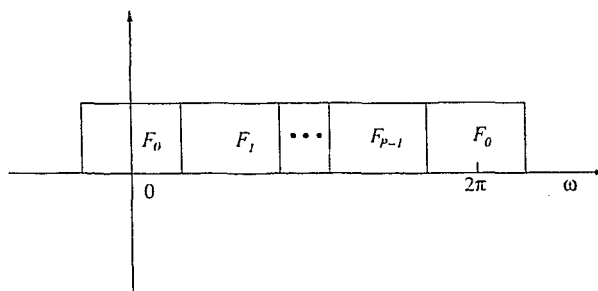


Figure 2.2: Ideal magnitude responses in a P -subchannel filter bank

According to the sampling theory, the original signal $x(n)$ can not be recovered perfectly from the signal $\hat{x}(n)$ if $K > P$. With $K \leq P$, $x(n)$ may be restored from $\hat{x}(n)$ if the filter bank satisfies the PR property.

2.1.1 Basic Building Blocks

Two of the most basic building blocks used in multirate filter bank systems are the decimator and the interpolator, which are shown in Fig. 2.1 with symbols $\downarrow K$ and $\uparrow K$, respectively. The K -fold decimator takes an input sequence $x(n)$ and retains only samples that occur at times which are multiples of K . Fig. 2.3 demonstrates the idea for $K = 2$. The input/output relation is therefore $y(n) = x(Kn)$.

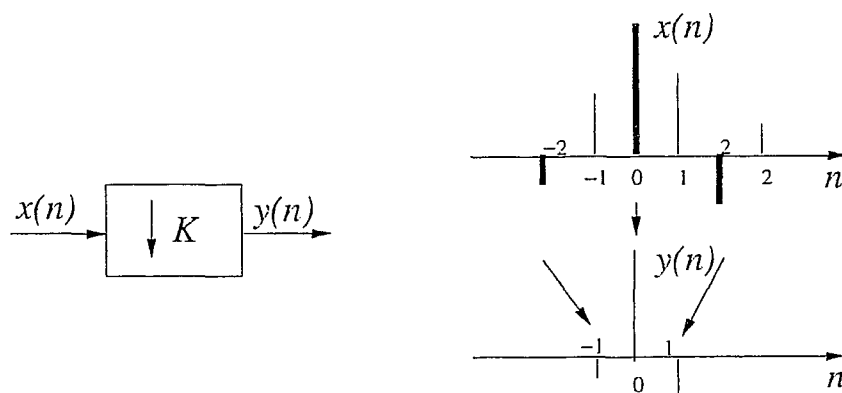


Figure 2.3: Demonstration of decimation for $K = 2$

The relation of the input $x(n)$ and output $y(n)$ of a K -fold decimator, which denoted

as $\downarrow K$, in Z -transform domain is

$$Y(z) = [X(z)]_{\downarrow K} = \frac{1}{K} \sum_{l=0}^{K-1} X(z^{1/K} W^l), \quad (2.1)$$

where W is defined as $W = e^{-j2\pi/K}$. With $z = e^{j\omega}$, Eq. (2.1) becomes

$$Y(e^{j\omega}) = \frac{1}{K} \sum_{l=0}^{K-1} X(e^{j(\omega-2\pi l)/K}), \quad (2.2)$$

which shows that $Y(e^{j\omega})$ is a sum of K uniformly shifted versions of an K -fold stretched version of $X(e^{j\omega})$. There are overlaps between various terms in Eq. (2.2) and these overlaps are usually called aliasing.

The K -fold interpolator, indicated by the symbol of $\uparrow K$, has the following input-output relationship:

$$y(n) = \begin{cases} x(\frac{n}{K}), & \text{if } n \text{ is multiples of } K, \\ 0, & \text{otherwise,} \end{cases} \quad (2.3)$$

i.e., the output $y(n)$ of the interpolation is obtained by inserting $K-1$ zero-valued samples between the adjacent samples of $x(n)$. Fig. 2.4 is a demonstration of this operation for $K=2$.

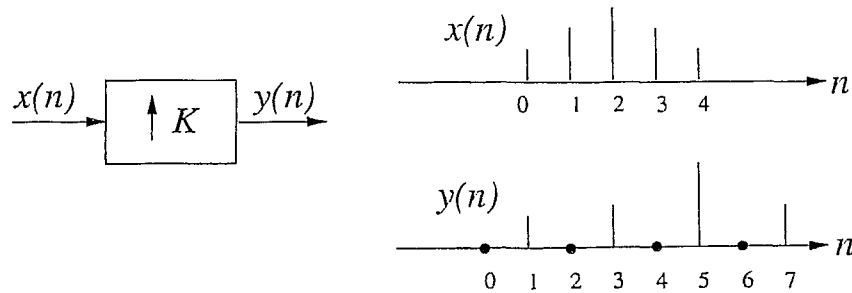


Figure 2.4: Demonstration of the interpolator for $K=2$.

In the transform domain the input-output relationship of an interpolator, expressed with $\uparrow K$, is equivalent to

$$Y(z) = [X(z)]_{\uparrow K} = X(z^K) \quad \text{or} \quad Y(e^{j\omega}) = X(e^{j\omega K}), \quad (2.4)$$

i.e., $Y(e^{j\omega})$ is merely a K -fold compressed version of $X(e^{j\omega})$. Since $X(e^{j\omega})$ is periodic with period 2π , the function $Y(e^{j\omega})$ has period of $2\pi/K$.

As shown in Fig. 2.1, the filter preceding a (K -fold) decimator, $H_p(z)$, $k = 0, 1, \dots, P-1$, is called a decimation filter. A decimation filter is used to bandlimit the signal and reduce the aliasing effect caused by the decimator. On the other hand, an interpolation filter $F_p(z)$, $k = 0, 1, \dots, P-1$, follows an interpolator to eliminate the repetitions of the compressed version of $u_k(e^{j\omega})$ caused by the interpolator. In time domain, the input-output relation of a decimation filter can be expressed as:

$$u_p(n) = \sum_{l=-\infty}^{\infty} x_p(l)h_p(nK-l) = \sum_{l=-\infty}^{\infty} h_p(l)x_p(nK-l), \quad (2.5)$$

for $p = 0, 1, \dots, P-1$, and the input-output relation of an interpolation filter can be expressed as:

$$\hat{x}_p(n) = \sum_{l=-\infty}^{\infty} u_p(l)f_p(n-Kl). \quad (2.6)$$

2.1.2 Polyphase Structures

The polyphase representation is important in the analysis and implementation of multirate filter bank systems because it permits great simplification of theoretical results and also leads to computationally efficient implementations of decimation/interpolation filters, as well as filter banks. In the following, the discussion is limited to the maximally decimated filter banks of which the number of subbands equals to upsampling/downsampling factor, i.e. $K = P$. In the following, the letter P is used to represent both the number of subbands and the upsampling/downsampling factor.

To explain the basic idea of the polyphase structure, let $H(z)$ be any transfer function with impulse response $h(n)$. Define the P sequences

$$e_l(n) = h(l + Pn), \quad 0 \leq l \leq P-1, \quad (2.7)$$

and define

$$E_l(z) = \sum_{n=-\infty}^{\infty} e_l(n)z^{-n}, \quad (2.8)$$

then $H(z)$ can be expressed as

$$H(z) = \sum_{l=0}^{P-1} z^{-l} E_l(z^P). \quad (2.9)$$

As defined in Eq. (2.8), $\{E_0(z), E_1(z), \dots, E_{P-1}(z)\}$ are said to be the P polyphase components of $H(z)$ and Eq. (2.9) is called the (P -component) polyphase representation of $H(z)$. A second type of polyphase representation is of the form $H(z) = \sum_{l=0}^{P-1} z^{-(P-1-l)} R_l(z^P)$, where $R_l(z) = E_{P-1-l}(z)$ are permutations of $E_l(z)$. The latter representation is more convenient in dealing with synthesis filters.

Two useful identities about polyphase structure, so called noble identities, are introduced in Fig. 2.5, while symbol ' \equiv ' means two items in both sides of the symbol are equivalent. These identities hold for any $H(z)$. Please refer to [26] for proofs of these identities.

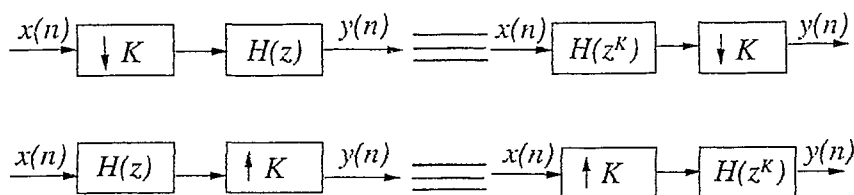


Figure 2.5: Noble identities of multirate systems

The filter banks in Fig. 2.1 can be simplified by applying polyphase structure. The analysis filters can be expressed as

$$H_p(z) = \sum_{l=0}^{P-1} z^{-l} E_{pl}(z^P), \quad (2.10)$$

where $E_{pl}(z^P)$ is the z -transform of $e_{pl}(n)$ which is defined as

$$e_{pl}(n) = h_p(l + Pn). \quad (2.11)$$

We can put the z -transform of analysis filters in matrix format as

$$\begin{bmatrix} H_0(z) \\ H_1(z) \\ \vdots \\ H_{P-1}(z) \end{bmatrix} = \mathbf{E}(z^P) \begin{bmatrix} 1 \\ z^{-1} \\ \vdots \\ z^{-(P-1)} \end{bmatrix}, \quad (2.12)$$

where

$$\mathbf{E}(z) = \begin{bmatrix} E_{00}(z) & E_{01}(z) & \cdots & E_{0,P-1}(z) \\ E_{10}(z) & E_{11}(z) & \cdots & E_{1,P-1}(z) \\ \vdots & \vdots & \ddots & \vdots \\ E_{P-1,0}(z) & E_{P-1,1}(z) & \cdots & E_{P-1,P-1}(z) \end{bmatrix}, \quad (2.13)$$

The set of synthesis filters can be expressed in a similar way with the second type of polyphase structure as

$$F_p(z) = \sum_{l=0}^{P-1} z^{-(P-1-l)} R_{lp}(z^P), \quad (2.14)$$

where $R_{lp}(z) = E_{l(P-1-l)}(z)$. Using matrix notations we have

$$\begin{bmatrix} F_0(z) & F_1(z) & \cdots & F_{P-1}(z) \end{bmatrix} = \begin{bmatrix} z^{-(P-1)} & z^{-(P-2)} & \cdots & 1 \end{bmatrix} \mathbf{R}(z^P), \quad (2.15)$$

where

$$\mathbf{R}(z) = \begin{bmatrix} R_{00}(z) & R_{01}(z) & \cdots & R_{0,P-1}(z) \\ R_{10}(z) & R_{11}(z) & \cdots & R_{1,P-1}(z) \\ \vdots & \vdots & \ddots & \vdots \\ R_{P-1,0}(z) & R_{P-1,1}(z) & \cdots & R_{P-1,P-1}(z) \end{bmatrix}, \quad (2.16)$$

By adopting above polyphase representations, the filter banks of Fig. 2.1 can be represented with a equivalent representation shown in Fig. 2.6. With noble identities shown in Fig. 2.5, Fig. 2.6 can be redrawn as in Fig. 2.7, where matrix $\mathbf{Q}(z) = \mathbf{R}(z)\mathbf{E}(z)$ is the transfer matrix. Polyphase representations can be used to explain the PR property which will be discussed in the following.

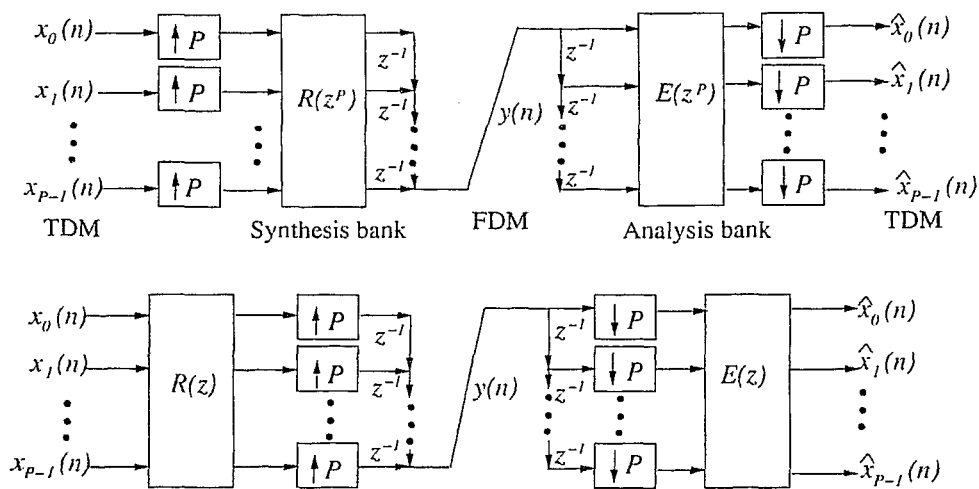


Figure 2.6: The polyphase representation of a P -band maximally decimated filter bank

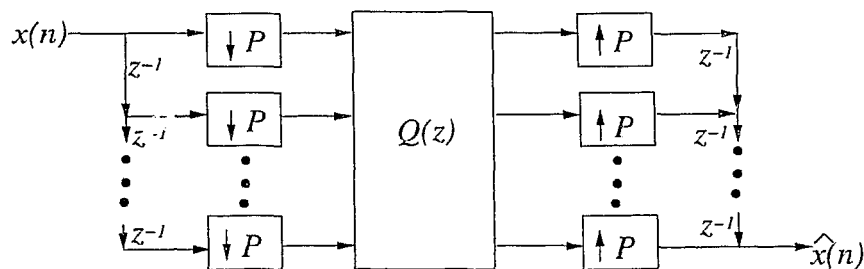


Figure 2.7: The simplification of polyphase representation of P -band maximally decimated filter bank

2.1.3 Perfect Reconstruction Property

When a QMF bank is free from aliasing, amplitude distortion and phase distortion, then the reconstructed signal $\hat{x}(n)$ is merely a scaled and delayed version of $x(n)$, i.e. $\hat{x}(n) = cx(n - m_0)$, where both c and m_0 are constants and m_0 is an integer, then this filter bank is said to have the PR property. The necessary and sufficient condition of the PR property for a maximally decimated QMF bank are

$$Q(z) = R(z)E(z) = cz^{-n_0}I, \quad (2.17)$$

or most generally,

$$Q(z) = R(z)E(z) = cz^{-n_0} \begin{bmatrix} 0 & I_{P-r} \\ z^{-1}I_r & 0 \end{bmatrix}, \quad (2.18)$$

for some integer r with $0 \leq r \leq P - 1$ and some integer n_0 . The I is the identity matrix. The delay involved in the filter bank is $m_0 = Pn_0 + r + P - 1$. Without loss of much generality, by omitting the effects of the constant delay and scaling and assigning the delay factor as $r = 1$, the necessary and sufficient condition for a filter bank to be PR can be written as

$$Q(z) = R(z)E(z) = I, \quad (2.19)$$

or

$$Q(z) = R(z)E(z) = \begin{bmatrix} 0 & I_{P-1} \\ z^{-1} & 0 \end{bmatrix}. \quad (2.20)$$

2.2 Filter Bank Based Transmultiplexer

The function of transmultiplexer in digital communications is to convert between two data formats called the TDM format and the FDM format. This function can be accomplished with a set of analysis filters and a set of synthesis filters.

2.2.1 TDM and FDM

To describe the TDM format consider Fig. 2.8(a), where three signals are passed through 3-fold interpolator and added through a delay chain. It can be shown that $y(n)$ is an interleaved version of the three signals, that is, it has the form

$$y(n) = \{\dots, x_0(0), x_1(0), x_2(0), x_0(1), x_1(1), x_2(1), \dots\}$$

This is the TDM version of the three signals. We can recover the three signals from $y(n)$ by using the time-domain demultiplexer shown in Fig. 2.8(b). To explain the FDM

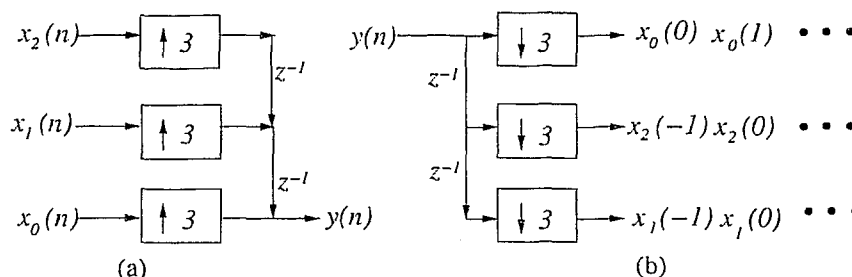


Figure 2.8: (a) Time domain multiplexing (b) Time domain demultiplexing.

operation, consider Fig. 2.9 where the frequency responses of three signals $x_0(n)$, $x_1(n)$ and $x_2(n)$ are shown. The FDM signal $y(n)$ is a single composite signal, whose transform $Y(e^{j\omega})$ is obtained by ‘pasting’ the frequency response of the individual signals next to each other. The FDM operation can be performed using the circuit shown at the right bottom of Fig. 2.9, where each individual signal is first passed through an interpolator to obtain a 3-fold compression of the transform. The interpolation filter $F_p(z)$ (assume ideal for this discussion), $p = 0, 1, 2$, retains one out of the three images which appear in $X_p(e^{j3\omega})$. The shaded portions in Fig. 2.9 are the retained images from each signal. The

filter responses, which pass the shaded regions of the respective signals, are shifted with respect to each other so that the retained parts from $X_p(e^{j3\omega})$ do not overlap with the retained parts from $X_k(e^{j\omega})$, $p \neq k$. When the outputs of the three filters are summed up, the FDM signal, $Y(e^{j\omega})$, is obtained.

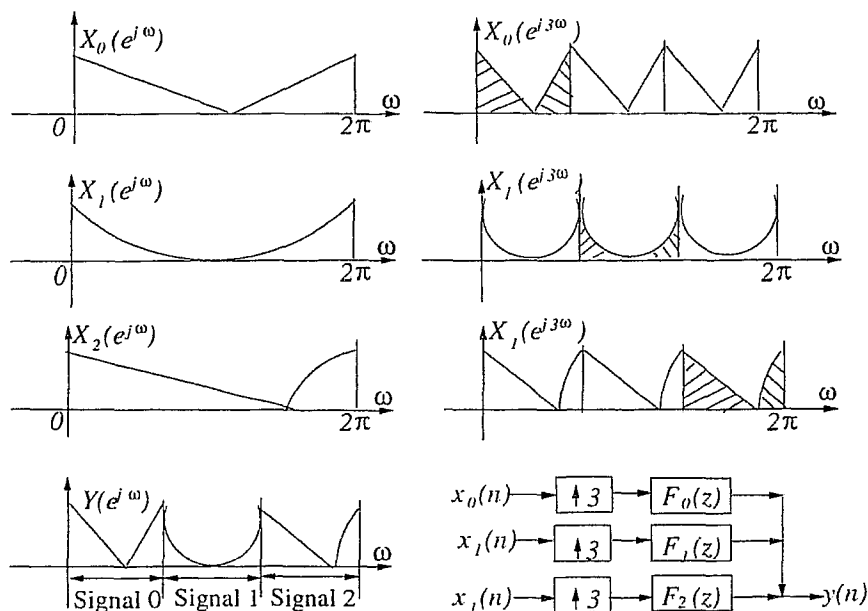


Figure 2.9: The operation of a frequency division multiplexer.

Fig. 2.10 shows the complete filter bank based transmultiplexer. When the synthesis filters, $\{F_0(z), F_1(z), \dots, F_{P-1}(z)\}$, are non-ideal, the adjacent spectra in Fig. 2.9 will actually tend to overlap. Similarly if the analysis filters, $H_p(z), p = 0, 1, \dots, P - 1$, are non-ideal, the output of $H_p(z), p = 0, 1, \dots, P - 1$, has contributions from $X_p(e^{j\omega})$ as well as $X_k(e^{j\omega})$ for $p \neq k$. Therefore in general, each of the reconstructed signals $\hat{x}_p(n)$ has contribution from the desired signal $x_p(n)$ as well as the 'cross-talk' terms $x_k(n), p \neq k$. In the following, we will present an approach to transmultiplexing in which cross-talk is permitted in the TDM \rightarrow FDM converter and then cancelled by the FDM \rightarrow TDM converter stage. It can be shown that the cross talk terms can be completely eliminated with carefully selected analysis and synthesis filters.

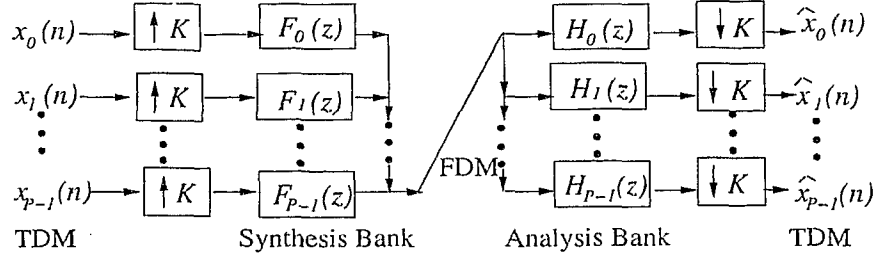


Figure 2.10: The transmultiplexer based on filter bank structure

2.2.2 Perfect Reconstruction Transmultiplexer

If the received signal $\hat{x}_p(n)$ of subchannel p , $p = 0, 1, \dots, P-1$, is just a delayed and scaled version of $x_p(n)$, then the transmultiplexer is a PR transmultiplexer. In the following, the sufficient condition for a PR transmultiplexer is summarized.

Fig. 2.10 shows that

$$\hat{X}_p(z) = \left[\sum_{k=0}^{P-1} X_k(z^P) F_k(z) H_p(z) \right]_{\downarrow P} = \sum_{k=0}^{P-1} X_k(z) [F_k(z) H_p(z)]_{\downarrow P} = \sum_{k=0}^{P-1} X_k(z) S_{kp}(z), \quad (2.21)$$

for $0 \leq k, p \leq P-1$, where $S_{kp}(z)$ is the polyphase component of $H_k(z)F_p(z)$. By defining

$$\mathbf{x}(n) = \begin{bmatrix} x_0(n) \\ \vdots \\ x_{P-1}(n) \end{bmatrix}, \quad (2.22)$$

and

$$\hat{\mathbf{x}}(n) = \begin{bmatrix} \hat{x}_0(n) \\ \vdots \\ \hat{x}_{P-1}(n) \end{bmatrix}, \quad (2.23)$$

Eq. (2.21) can be expressed more compactly as

$$\hat{\mathbf{X}}(z) = \mathbf{S}(z)\mathbf{X}(z). \quad (2.24)$$

i.e., the transmultiplexer is an linear time-invariant (LTI) system with transfer matrix $\mathbf{S}(z)$. The system is free from cross talk if and only if $\mathbf{S}(z)$ is a diagonal constant matrix. Without loss of generality, the sufficient condition for a PR transmultiplexer can be defined as

$$\mathbf{S}(z) = \mathbf{I}. \quad (2.25)$$

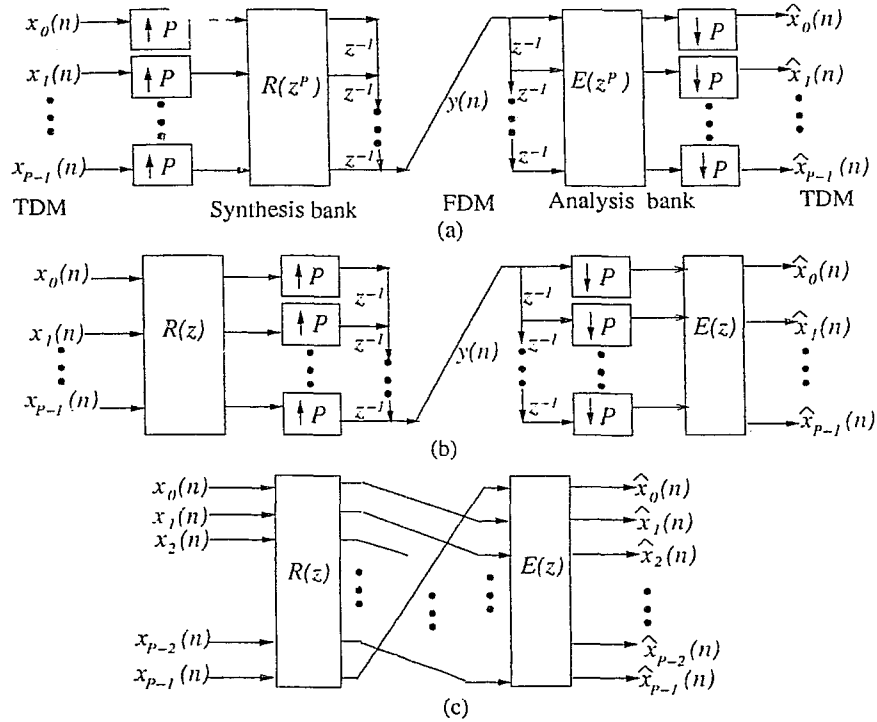


Figure 2.11: (a) Equivalent structures for the transmultiplexer using polyphase matrices, (b) rearrangement using noble identities, (c) simplified structure.

The relation between maximally decimated PR filter bank and maximally decimated PR transmultiplexer is summarized in the following. By using the polyphase decomposition for the transmultiplexer shown in Fig. 2.10, the resulting equivalent transmultiplexer circuit is shown in Fig. 2.11(a) and can be further simplified into the equivalent form shown in Fig. 2.11 (c). It is, therefore, clear that the transfer matrix $S(z)$ can be expressed as

$$S(z) = E(z)\Gamma(z)R(z), \quad (2.26)$$

where

$$\Gamma(z) = \begin{bmatrix} 0 & 1 \\ z^{-1}\mathbf{I}_{P-1} & 0 \end{bmatrix}. \quad (2.27)$$

The sufficient condition for a PR transmultiplexer can then be expressed with the transfer function of a QMF as

$$S(z) = I \Leftrightarrow E(z)\Gamma(z)R(z) = I \Leftrightarrow R(z)E(z) = \Gamma^{-1}(z). \quad (2.28)$$

Substituting for $\Gamma(z)$, this becomes

$$\mathbf{Q}(z) = \mathbf{R}(z)\mathbf{E}(z) = \begin{bmatrix} 0 & \mathbf{I}_{P-1} \\ z^{-1} & 0 \end{bmatrix}, \quad (2.29)$$

which is the sufficient and necessary condition for a QMF to have PR property which is described in section 2.1.3. Therefore, we can summarize the above results as follows: If $H_p(z)$ and $F_p(z)$, $p = 0, 1, \dots, P-1$, are the analysis and synthesis filters in a maximally decimated QMF bank satisfying the PR condition of Eq. (2.29), then the transmultiplexer, with synthesis bank $F_p(z)$, $p = 0, 1, \dots, P-1$ and analysis bank $H_p(z)$, $p = 0, 1, \dots, P-1$, is a PR transmultiplexer.

2.3 Summary

In this chapter, the fundamentals of digital filter banks and filter bank based transmultiplexers are summarized as presented in [10, 26, 28]. The operations of the decimator and interpolator are introduced. The functions of the analysis filter and synthesis filters are described. The polyphase presentation of a filter bank and the sufficient and necessary condition for a filter bank to be PR are presented. The TDM and FDM functions performed by a filter bank based transmultiplexer is demonstrated and the relationship between the PR filter bank and the PR transmultiplexer is derived. In the next chapter, the fundamentals of an OFDM system will be presented on the basis of the filter bank theory introduced in this chapter.

Chapter 3

Orthogonal Frequency Division Multiplexing (OFDM) Systems

AS one of the most important classes of MCM, OFDM is a modulation scheme that allows digital data to be efficiently and reliably transmitted over a radio channel, even in multipath environments. An OFDM system transmits data by using a large number of narrow bandwidth subcarriers, which are chosen in such a way that they do not interfere with each other. The name ‘OFDM’ is derived from the fact that the digital data is sent using many subcarriers, each of a different frequency (FDM) and these subcarriers are orthogonal to each other, hence orthogonal frequency division multiplexing [29].

The origins of the OFDM modulation started in the late 1960’s. In 1971 Weinstein [11] introduced the idea of using a DFT-based filter bank for implementation of the generation and reception of OFDM signals. In 1990’s, the DWMT modulation was proposed as an alternative of the DFT-based OFDM modulation [13]. The OFDM modulation has been adopted in many standards of current and future wireline and wireless applications, such as asymmetric digital subscriber line (ADSL), European digital audio broadcasting (DAB), European digital video broadcasting (DVB), short-range wireless access and wireless LAN standards (IEEE802.11a).

In this chapter, the basic principles of OFDM systems are introduced. Section 3.1 presents the data generation and modulation in OFDM modulation, characteristics of OFDM filter bank modulator and demodulator, and orthogonality of subchannels in

OFDM systems are presented. Section 3.2 explains two important realizations of the OFDM modulation, the DFT-based OFDM system and the DWMT system and the properties of both systems. Section 3.3 summarizes this chapter.

3.1 Basic Principles of OFDM

3.1.1 Data Generation and Modulation

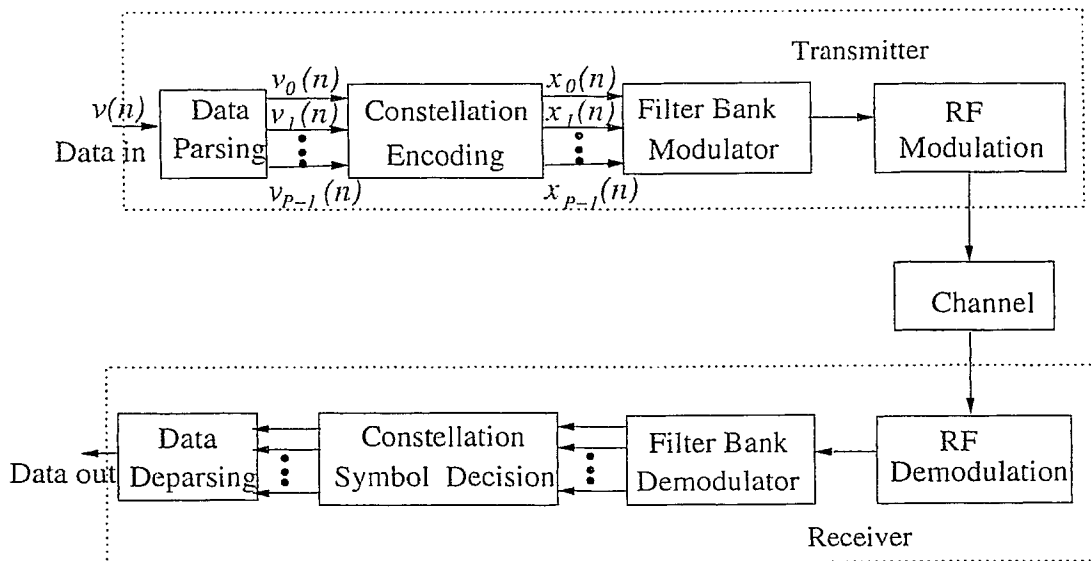


Figure 3.1: The block diagram for an OFDM transceiver

Fig. 3.1 shows a block-level diagram for an OFDM transceiver. The operation of an OFDM transceiver is outlined as follows. Since the data to be transmitted are typically in the form of a serial bit data stream (as $v(n)$ shown in Fig. 3.1), a data parsing stage is needed to convert the input serial bit stream to the symbols to be transmitted over subchannels. Fig. 3.2 shows operation details of data parsing [10].

As shown in Fig. 3.2, $v(n)$ represents the binary data stream to be transmitted over a transmission channel and it is divided into non-overlapping b -bit segments, which are then partitioned into P groups $v_0(n), v_1(n), \dots, v_{P-1}(n)$. The group $v_p(n)$ consists of b_p bits, $p = 0, 1, \dots, P - 1$. The time interval between $v_p(n)$ and $v_p(n + 1)$ is b times longer

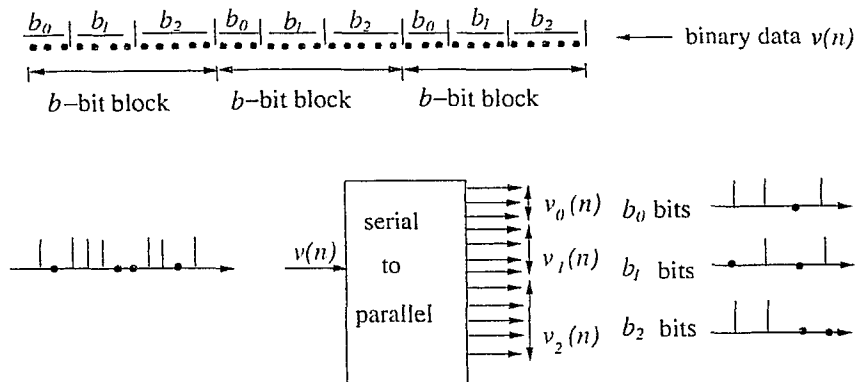


Figure 3.2: Data parsing function in an OFDM transceiver. The number of subchannels $P = 3$. Sign ‘.’ represents single binary symbol

than that between $v(n)$ and $v(n + 1)$. This longer symbol times provide better immunity to impulse noise.

Each binary data group generated by the parsing stage, $v_p(n)$, $p = 0, 1, \dots, P - 1$, are encoded separately using various discrete coding schemes. One of the typical modulation schemes in an OFDM system is the MPSK modulation. The alphabet size (for example, BPSK or 16-PSK) of the modulation scheme for a subchannel is chosen to be the maximum that the subchannel, on which the coded symbols are to be transmitted, can support with an acceptable symbol error rate. In an OFDM system, the channel is divided into a number of narrow band subchannels. A subchannel which is affected by the narrowband interference can be identified easily, the alphabet size for that subchannel can be made small, or the use of the subchannel can be inhibited.

The output of the constellation encoding block, $x_0(n), x_1(n), \dots, x_{P-1}(n)$, are modulation symbols for the filter bank modulator. In the OFDM transmission, time is divided into continuous, non-overlapping frames, and during the frame n , P symbols, $x_0(n), x_1(n), \dots, x_{P-1}(n)$, with each one modulated to one of P subchannels, are transmitted in parallel. The output of the filter bank modulator, a serial data stream of the FDM format, is modulated on a radio frequency (RF) carrier and transmitted through the transmission channel. At the receiver end, filter bank demodulator receives the composite data stream and time-division multiplexes them into P parallel data streams. After all received sym-

bols have been decoded, the parallel data streams are converted into the serial binary data stream in an inversive way of parsing function at the transmitter end. The combination of the pair of the OFDM filter bank modulator and demodulator is referred as an OFDM transmultiplexer.

3.1.2 OFDM Transmultiplexer

An OFDM transmultiplexer is a transmultiplexer based on filter bank structure, which is introduced in section 2.2. Fig. 3.3 shows the block diagram of the OFDM modulator and demodulator, or the OFDM transmultiplexer, and the communication channel.

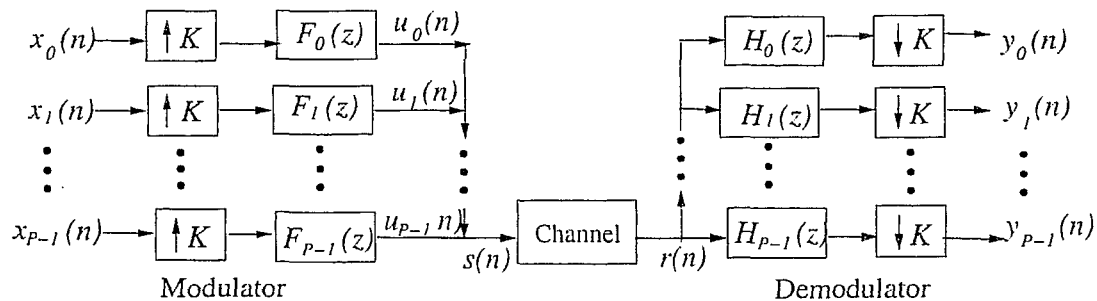


Figure 3.3: The block diagram of an OFDM transmultiplexer

Operation of OFDM Transmultiplexer

The operation of an OFDM transmultiplexer can be described as follows. The output of the modulation filter of subchannel p , $F_p(z)$, $0 \leq p \leq P - 1$, has the format

$$u_p(n) = \sum_{i=-\infty}^{\infty} x_p(i) f_p(n - iK). \quad (3.1)$$

Fig. 3.4 demonstrates how this construction is done in time domain for the 0-th filter $f_0(n)$, which we assume to be a lowpass filter. Essentially one copy of the impulse response sequence $f_0(n)$ is drawn around every sample of $x_0(n)$ (separated by K) and all copies are summed up. If the length of $f_0(n)$ is not greater than K , there will be no overlap in $u_0(n)$. Outputs from all modulation filters, $\{u_0(n), u_1(n), \dots, u_{P-1}(n)\}$, are added up to form the composite signal $s(n)$ to be transmitted through the transmission channel. At the receiver, the filter bank demodulator separates the signal $r(n)$ into the components $y_p(n)$,

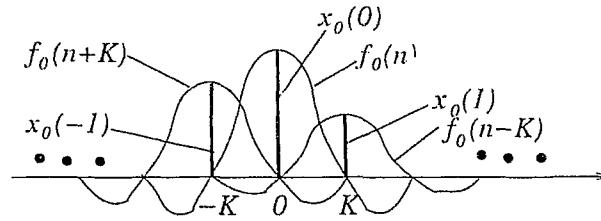


Figure 3.4: The construction of output of transmitting filters

which are distorted and noisy versions of the symbols $x_p(n)$, $0 \leq p \leq P - 1$. The task at this point is to detect the symbols $x_p(n)$ from $y_p(n)$ with acceptable error probability, thus the crucial issue in OFDM transmission is to make $y_p(n)$ resemble $x_p(n)$.

Property of OFDM Modulation and Demodulation Filters

In the ideal case, which means no distortion and noise in the channel, $x_p(n)$ should be perfectly retrieved from $y_p(n)$, $p = 0, 1, \dots, P - 1$, therefore the modulation and demodulation filters should satisfy the PR property which is expressed in Eq. (2.25). This PR property can be alternatively expressed in time domain as:

$$\sum_l f_{p_1}(l) h_{p_2}(Kn - l) = \delta(p_1 - p_2) \delta(n), \quad (3.2)$$

where $0 \leq p_1, p_2 \leq P - 1$, $\delta(p_1 - p_2)$ and $\delta(n)$ are the Kronecker functions.

For OFDM systems, P subchannels are selected to be mutually orthogonal, which means they are mutually independent of each other, or mathematically, the inner product of each pair of subchannel impulse response sequences is zero. Orthogonality is the essential property of an OFDM system since it allows multiple information signals to be transmitted over a common channel and each signal can be detected with a negligibly small amount of interference from the other signals, if the channel distortion is mild compared to the bandwidth of a subchannel. The orthogonality between each pair of subchannels can be expressed in time domain as

$$\sum_n f_{p_1}(l) f_{p_2}^*(l - Kn) = \delta(p_1 - p_2) \delta(n), \quad (3.3)$$

where $0 \leq p_1, p_2 \leq P - 1$.

The equivalent expression of Eq. (3.3) in frequency domain can be written as

$$\frac{1}{K} \sum_{k=1}^{K-1} H_{p_1}\left(\frac{\omega - 2\pi k}{K}\right) H_{p_1}^*\left(\frac{\omega - 2\pi k}{K}\right) = \delta(p_1 - p_2). \quad (3.4)$$

Eq. (3.3) also guarantees that each modulation filter, $f_p(n)$, $p = 0, 1, \dots, P - 1$, has unit energy. When all subchannels are mutually orthogonal as expressed in with Eq. (3.3), the PR can be fulfilled by making the relation between the modulation and demodulation filters as

$$h_p(l) = f_p^*(-l), \quad (3.5)$$

where $0 \leq p \leq P - 1$.

From Eq. (3.5), it can be concluded that when modulation filters are mutually orthogonal and have unit energy, i.e., modulation filters are orthonormal, the demodulation filters are orthonormal as well.

Fading channels, which are multipath and frequency selective, always destroy the orthogonality of subchannels. As a consequence, the received subchannel symbols $y_p(n)$, $0 \leq p \leq P - 1$ are distorted by both ISI and ICI introduced by the fading channel.

3.2 DFT-Based OFDM and DWMT

The DFT-based OFDM system and the DWMT system are two important realizations of OFDM systems. The former is the most well known OFDM system and it has been thoroughly investigated in [5, 6, 8, 29, 30].

3.2.1 DFT-based OFDM

The idea of using the inverse DFT (IDFT) and DFT transforms for the generation and reception of OFDM signals was proposed by Weinstein and Ebert several decades ago [11]. This approach presents an opportunity for an easy implementation of OFDM, especially with the use of Fast Fourier Transform (FFT), which is an efficient implementation of DFT. The IDFT and DFT transforms can be implemented with an IDFT filter bank and a DFT filter bank, respectively [8, 14].

The construction of IDFT filter bank can be divided into two steps. Firstly the low pass modulation filter is chosen as a P -long rectangular pulse

$$f_0(l) = \begin{cases} \frac{1}{\sqrt{P}}, & 0 \leq l \leq P-1, \\ 0, & \text{otherwise,} \end{cases} \quad (3.6)$$

and then the other $P-1$ modulation filters are obtained by rotating the low pass filter as

$$f_p(l) = f_0(l)e^{j\omega_p l}, \quad (3.7)$$

where $\omega_p = 2\pi p/P$. We can see that, the frequency response of the $P-1$ band pass transmitting filters $\{F_1(e^{j\omega}), F_2(e^{j\omega}), \dots, F_{P-1}(e^{j\omega})\}$ are obtained by shifting the frequency response of the low pass filter $F_0(e^{j\omega})$, i.e.

$$F_p(e^{j\omega}) = F_0(e^{j\omega - 2\pi p/P}), \quad i = 1, \dots, P-1, \quad (3.8)$$

and all filters $\{f_0(n), f_1(n), \dots, f_{p-1}(n)\}$ are of same length $L = P$.

The OFDM modulation with filters defined in Eqs. (3.6) and (3.7) can also be described with matrix operations. Denoting the IDFT matrix Φ as

$$\Phi_{P \times P} = \begin{bmatrix} f_0(0) & f_0(1) & \dots & f_0(P-1) \\ f_1(0) & f_1(1) & \dots & f_1(P-1) \\ \vdots & \vdots & \dots & \vdots \\ f_{P-1}(0) & f_{P-1}(1) & \dots & f_{P-1}(P-1) \end{bmatrix}, \quad (3.9)$$

and vector \mathbf{X} as

$$\mathbf{X} = \begin{bmatrix} x_0(n) \\ x_1(n) \\ \vdots \\ x_{P-1}(n) \end{bmatrix}, \quad (3.10)$$

the output of the IDFT filter bank modulator, which is denoted as $\mathbf{U} = [u_0(n), u_1(n), \dots, u_{P-1}(n)]^T$, can be obtained by

$$\mathbf{U} = \mathbf{X} \cdot \Phi. \quad (3.11)$$

The orthogonormality of the IDFT filter bank follows the fact that the IDFT matrix Φ is unitary, i.e., $\Phi\Phi^H = \mathbf{I}$, where \mathbf{I} is the identity matrix. Eq. (3.5) holds to make the filter bank modulator and demodulator fulfill the PR property.

In a DFT-based OFDM system, a subchannel has significant spectral overlap with a large number of its neighboring subchannels. Fig. 3.5 shows the frequency responses for the subchannels, which occupying frequency range $[0, 0.14]$, of a DFT-based OFDM system with $P = 32$ subchannels. It shows that the first sidelobe is as high as -13 dB. The intensive spectral overlaps of adjacent subchannels in DFT-based OFDM systems indicate the subchannel isolation can only be retained for channels which have virtually no distortion.

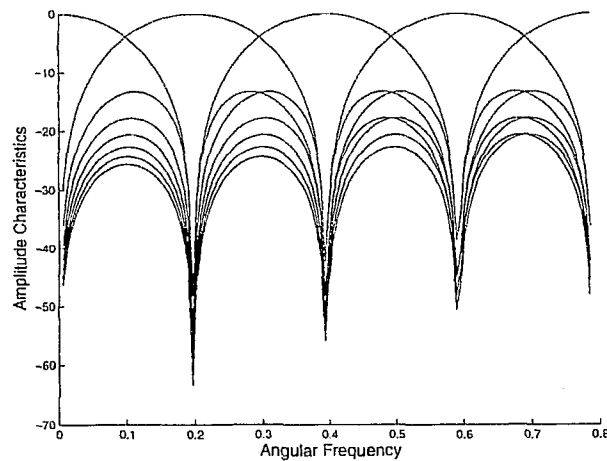


Figure 3.5: Subchannel frequency responses of DFT-based OFDM system for $\omega \in [0, 0.88]$ and $P = 32$

To compensate for the high degree of spectral overlaps, a technique in which a 'cyclic prefix' (CP) being inserted at the beginning of each transmission block, which consisting of P symbols, was proposed. The CP can be the trailing zeroes (a null signal), which is referred as the zero-padded CP, or a part of the signal block as shown in Fig. 3.6. At the receiver end, the CP is discarded to avoid interblock interference and each truncated block is demodulated with a DFT filter bank. With the inclusion of the CP, the following rule holds: If the channel impulse response is shorter than the length of the CP, L_k , the subchannel isolation is achieved [30]. However, for fixed symbol alphabet sizes, the inclusion of the CP reduces the transmission rate by the fraction of $P/(P + L_k)$ [13].

Theoretically, the inclusion and removal of zero-padded cyclic prefix can be accom-

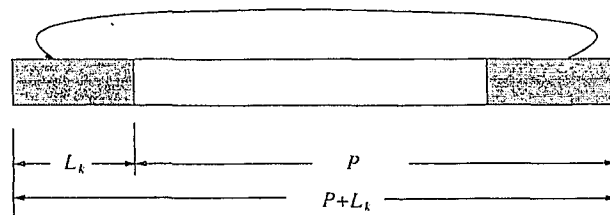


Figure 3.6: The stylized plot of CP inclusion. The l_k long CP can also be the trailing zeroes.

plished by choosing upsampling/downsampling factor as $K = L + L_k$ and modulation filters in Fig. 3.3 as [13]

$$h_p(l) = \begin{cases} 0, & -P - L_k + 1 \leq l \leq -P, \\ f_p^*(-l), & -P + 1 \leq l \leq 0. \end{cases} \quad (3.12)$$

DFT-based OFDM systems with CP is implemented as schematically shown in Fig. 3.7.

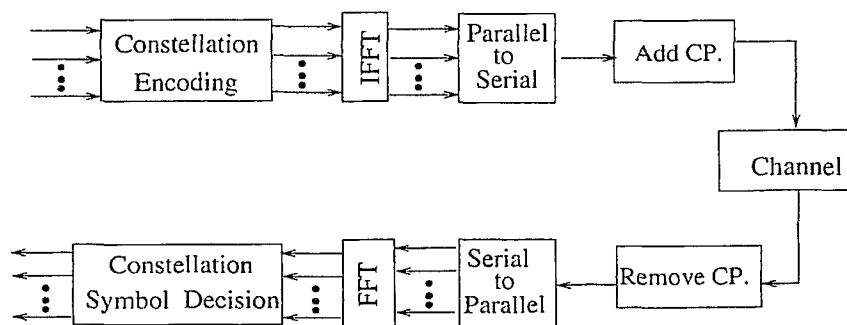


Figure 3.7: The schematic diagram of a DFT-based OFDM system

3.2.2 Discrete Wavelet Multitone Systems

The DWMT, or the overlapped discrete multitone, is an alternative form of OFDM transmission and it is proposed recently by Sandberg [13]. A DWMT system incorporates careful pulse design to achieve a high level of subchannel spectral containment, without sacrificing the PR property of the set of subchannels. The advantages introduced by the spectral containment properties of DWMT subchannels are that, the DWMT system is better able than the DFT-based OFDM system to ameliorate the effects of narrowband

interference and narrow band channel noise [2, 13], and do not need CP to separate transmitted data blocks for better error performance with compromised system efficiency. In a DWMT system, upsampling/downsampling factor $K = P$.

In DWMT systems, modulation filters are a set of real-valued cosine modulated filters which are generated from a prototype low pass filter $w(n)$ with the extended lapped transforms (ELT) [15, 31, 32, 33].

$$f_p(n) = w(n) \sqrt{\frac{2}{P}} \cos \left[\frac{\pi}{K} \left(p + \frac{1}{2} \right) \left(n + \frac{P+1}{2} \right) \right]. \quad (3.13)$$

There are two constraints for $w(n)$. Firstly the modulation filters generated with Eq. (3.13) should be mutually orthogonal, secondly the modulation filters and demodulation filters constructed with Eq. (3.5) should satisfy the PR property to make the system a PR system. Under these two constraints, $w(n)$ must fulfill the requirement expressed as [15], [33]):

$$\sum_{m=-\infty}^{\infty} w(n - mP)w(n + nP + 2rP) = \delta(r), \quad (3.14)$$

i.e., as long as $w(n)$ satisfies Eq. (3.14), the filters generated with Eqs. (3.13) and (3.5) can be employed respectively as modulation and demodulation filters of a DWMT system. It is shown that even with the enforcement of the PR condition in Eq. (3.14), there are enough degrees of freedom in choosing the lengths of modulation filters, and there are flexible combinations of transition width and stopband attenuation for subchannels.

Usually in DWMT systems, the length of $w(n)$, L , is chosen to be $L = gP$, $g \geq 2$ is the overlapping factor. In the DWMT transmission, each symbol in the g frames, $n, n-1, \dots, n-g+1$, contributes to the data segment that is transmitted during frame n .

Since there are more than one choice of $w(n)$ for each specific g , the one with the biggest mainlobe energy is usually chosen for the DWMT system. A good choice of $w(n)$ for $g = 2$ is [32]:

$$w(n) = \sin \left[\frac{\pi}{2P} \left(n + \frac{1}{2} \right) \right]. \quad (3.15)$$

The frequency responses of several subchannels, which are constructed with prototype filter $w(n)$ defined in Eqs. (3.15) and (3.13), are shown in Fig. 3.8 for a DWMT system

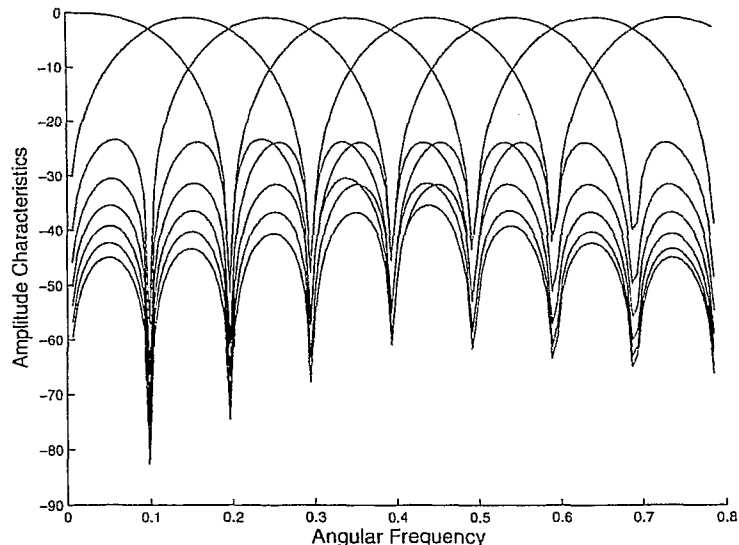


Figure 3.8: Frequency responses of a DWMT system for $\omega \in [0, 0.88]$ and $P = 32$

with $P = 32$ subchannels. From Fig. 3.8 we can see that the first side lobe of subchannels in the DWMT system is about 25 dB down from the main lobe and each subchannel occupies just the half the bandwidth which is occupied by the subchannels in the DFT-based OFDM with same number subchannels, as shown in Fig. 3.5. Generally for a DWMT system, with g getting larger, higher spectral concentration and tight subchannel spectral containment can be obtained.

3.3 Summary

In this chapter, the fundamentals of a generic OFDM system are presented. The data generation and modulation in an OFDM system, the mutual orthogonality of subchannels and the properties of modulation filters and demodulation filters of an OFDM system are introduced. The effect of fading channels on an OFDM system is explained. The properties and implementations of two special OFDM systems, namely DFT-based OFDM and DWMT systems, are presented as well.

Chapter 4

Symbol Error Rate Evaluation and Filter Bank Design for OFDM Systems with MPSK Modulation

As explained in chapter 3, the orthogonality among subchannels of an OFDM system is often destroyed by fading channels. As a result, the received signal of each subchannel is distorted by not only the channel noise, but ICI and ISI. The existence of the large amount of interference makes it difficult to theoretically evaluate the error performance of an OFDM system. Recently some attempts have been made to investigate the error performance of the DFT-based OFDM systems based on certain assumptions and bounds [6, 17, 18, 19, 20, 21, 34]. However, the error performance of a *generic* OFDM system, which fulfills both the perfect reconstruction (PR) and the orthogonality properties, as expressed in Eqs. (3.2) and (3.3) respectively, has not been systematically studied.

In this chapter, the error performance of a generic OFDM system, with the DFT-based OFDM system and the DWMT system as two realizations, is studied by considering the effects of both ISI, ICI and the additive channel noise. By investigating the expressions of a received symbol and interference involved in the received symbol to be decoded, and modelling the sum of ISI and ICI as a Gaussian random process, the probability density function (PDF) of the received symbol is derived. A closed-form symbol error rate (SER) expression is formulated for an OFDM system with MPSK modulation and the optimal

phase detector for each of the subchannels. Numerical Monte-Carlo simulations have been performed to verify the derived SER formula and simulation results demonstrate the consistency with the theoretical analysis, for both the DFT based OFDM systems and the conventional DWMT systems.

The derived SER formula can be used to evaluate both the DFT-based OFDM systems, no matter with or without CP, and the DWMT systems. It can also be employed as a criterion to design an OFDM system to obtain satisfactory error performance. By using this formula as the objective function, a novel OFDM system based on designed complex-valued unitary filter banks is presented in order to improve the error performance. Unlike to filters with real-valued, complex-valued filters have asymmetric frequency responses and are more suitable to deal with complex-valued signals which are often present in a wireless system. The filters of the designed unitary filter banks are inherently orthogonal. By parameterizing the coefficient of the complex-valued unitary filter banks with free parameters, it is possible to adjust the OFDM system for various design criterions. In this chapter, the derived SER formula is taken as the objective function, the complex-valued filter banks are designed to minimize the SER. Simulation results show that the new OFDM system based on designed filter banks outperforms the DWMT system in terms of SER, and its SER performance is comparable to that of the DFT-based OFDM system with CP, which is less efficient in terms of transmission rate.

The remainder of this chapter is organized as follows: In Section 4.1, a closed-form SER formula for a generic OFDM modulated with MPSK scheme is derived and its performance over AWGN channels and fading channels is investigated. In Section 4.2, a novel OFDM system based on complex-valued unitary filter banks, which can be adjusted to different design criterions, is presented. System simulations are described in Section 4.3 to verify the theoretical analysis about the SER performance, and to demonstrate the SER performance of designed OFDM systems. Section 4.4 summarizes this chapter.

4.1 Symbol Error Rate Evaluation for OFDM Systems with MPSK Modulation

4.1.1 System Modelling

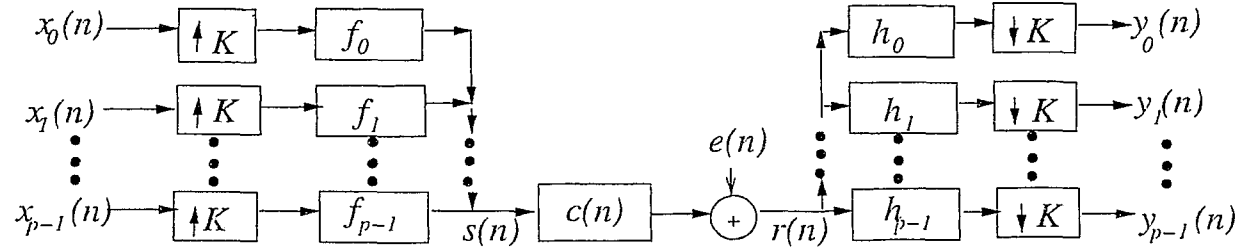


Figure 4.1: Block diagram for filter bank modulator and demodulator in OFDM systems

The filter bank based modulator and demodulator, with P subchannels, of a generic OFDM system are illustrated in Fig. 4.1. The modulation and demodulation filters of subchannel p , $0 \leq p \leq P - 1$, are denoted respectively as f_p and h_p , which are of length $L = gK$, where g is the overlapping factor, and K is the upsampling/downsampling factor. The modulation filters f_p , $0 \leq p \leq P - 1$, fulfill the orthogonality property (Section 3.1.2), i.e., for $0 \leq p_1, p_2 \leq P - 1$

$$\sum_{l=0}^{L-1} f_{p_1}(l) f_{p_2}^*(l - nK) = \delta(n) \delta(p_1 - p_2). \quad (4.1)$$

Moreover, the modulation and demodulation filters satisfy the PR property defined as

$$\sum_{l=0}^{L-1} f_{p_1}(l) h_{p_2}(nK - l) = \delta(n) \delta(p_1 - p_2). \quad (4.2)$$

Both DFT-based OFDM and DWMT systems are special cases of a generic OFDM system. For DFT-based OFDM, the low pass modulation filter is chosen as (section 3.2.1)

$$f_0(l) = \begin{cases} \frac{1}{\sqrt{P}}, & 0 \leq l \leq L - 1, \\ 0 & \text{otherwise} \end{cases} \quad (4.3)$$

Then the other $P - 1$ modulation filters are obtained by rotating the low pass filter to

$$f_p(l) = f_0(l) e^{j\omega_p l}, \quad (4.4)$$

where $\omega_p = 2\pi p/P$, $p = 1, \dots, P-1$. The inclusion of zero-padded CP can be implemented by choosing the upsampling/downsampling factor $K = P + L_k$, where L_k is the length of the CP and it is no shorter than the length of the transmission channel $c(n)$. Demodulation filters are generated as follows to remove the CP that is added at the transmitter end

$$h_p(l) = \begin{cases} 0 & -P - L_k + 1 \leq l \leq -P, \\ f_p^*(-l) & -P + 1 \leq l \leq 0. \end{cases} \quad (4.5)$$

For DFT-based OFDM, the overlapping factor $g = 1$. The length of filters for a DFT-based OFDM system with CP is $L = P + L_k$.

For a conventional real-valued cosine modulated filter bank based DWMT system, $K = P$ and modulation filters are generated as (section 3.2.2)

$$f_p(l) = w(l) \sqrt{\frac{2}{P}} \cos \left[\left(p + \frac{1}{2} \right) \left(l + \frac{P+1}{2} \right) \frac{\pi}{P} \right], \quad (4.6)$$

for $p = 0, 1, \dots, P-1$, and $w(l)$ is the impulse response of a low-pass filter, which is of length $L = gP$, $g \geq 2$. The demodulation filters of a DWMT system can be obtained by

$$h_p(l) = f_p(-l), \quad -L + 1 \leq l \leq 0. \quad (4.7)$$

The transmission channel $c(n)$ is modelled as a linear time invariant (LTI) FIR (finite impulse response) filter¹ of length L_c , followed by a stationary zero-mean random Gaussian noise source $e(n)$, which is independent of transmitted symbols $\{x_p(n), p = 0, 1, \dots, P-1\}$.

For an OFDM system with MPSK modulation scheme, abbreviated as an MPSK-OFDM system, a conventional optimal phase detector is employed for each subchannel to calculate the phase of each received symbol and decode the received symbol with preset phase boundaries. The SER for a generic MPSK-OFDM system is derived in the following.

4.1.2 Symbol Error Rate for Generic MPSK-OFDM Systems

In OFDM systems, at each time frame n_1 , P parallel symbols $\{x_0(n_1), x_1(n_1), \dots, x_{P-1}(n_1)\}$ are transmitted, with each symbol modulated to one of the P subchannels. The transmit-

¹ $c(n)$ can be considered as the overall transfer function resulting from the real communication channel and a time domain equalizer (TEQ), which precedes the filter bank demodulator in cases where a TEQ is employed.

ted subchannel symbol in subchannel p_1 at frame n_1 , $x_{p_1}(n_1)$, represents as well constellation points generated by a modulation scheme such as MPSK. Corresponding to each transmitted constellation point, $x_{p_1}(n_1)$, there is a received symbol $y_{p_1}(n_1 + d)$, where d is the system delay. If only the delay involved in the convolution with the modulation filter and demodulation filter, both of length $L = gK$, is considered, then $d = g$. The following formulation gives the expression of $y_{p_1}(n_1 + d)$.

Formulation 1: In an OFDM system shown in Fig. 4.1, assume the channel impulse response is $c(n)$, $n = 0, 1, \dots, L_c - 1$, and the zero-mean additive Gaussian random noise is $e(n)$. Then, for a given subchannel p_1 , the received symbol $y_{p_1}(n_1 + d)$, corresponding to the symbol $x_{p_1}(n_1)$ which transmitted at time frame n_1 , can be expressed as:

$$y_{p_1}(n_1 + d) = \bar{y}_{p_1} + \xi + \zeta, \quad (4.8)$$

where \bar{y}_{p_1} is the contribution from symbol $x_{p_1}(n_1)$, ξ is the contribution from channel noise, and ζ is the interference calculated by summing up all ICI and ISI items. Note that $x_{p_1}(n_1)$ is the only transmitted symbol contributing to \bar{y}_{p_1} , which can be expressed as follows

$$\bar{y}_{p_1} = \alpha_{p_1 p_1}(n_1) x_{p_1}(n_1), \quad (4.9)$$

ξ can be calculated as

$$\xi = \sum_{n=-\infty}^{\infty} e(n) h_{p_1}(n_1 K - n), \quad (4.10)$$

and ζ can be calculated as

$$\zeta = \sum_{n=-\infty}^{\infty} \sum_{p \neq p_1, p=0}^{P-1} \alpha_{pp_1}(n) x_p(n) + \sum_{n \neq n_1, n=-\infty}^{\infty} \alpha_{p_1 p_1}(n) x_{p_1}(n). \quad (4.11)$$

In Eqs. (4.9) and (4.11), $\alpha_{pp_1}(n)$, for $0 \leq p, p_1 \leq P - 1$, is the weight of the contribution from the transmitted symbol $x_p(n)$ to the received symbol $y_{p_1}(n_1 + d)$, and it is calculated as:

$$\alpha_{pp_1}(n) = \sum_{j=0}^{L_c-1} c(j) \sum_{l=0}^{L-1} f_p(l) h_{p_1}[(n_1 - n)K - j - l], \quad (4.12)$$

where L_c is the length of the channel $c(n)$.

Proof: As shown in Fig. 4.1, the composite data sequence to be transmitted over channel, $s(n)$, is the sum of the output signals of all modulation filters, i.e.

$$s(n) = \sum_{p=0}^{P-1} \sum_{i=-\infty}^{\infty} x_p(i) f_p(n - iK). \quad (4.13)$$

At the receiving end, the received signal $r(n)$ is distorted by channel noise and interference due to the non-ideal channel. $r(n)$ can be expressed as:

$$r(n) = s(n) * c(n) + e(n) = \sum_{k=-\infty}^{\infty} s(k) c(n - k) + e(n), \quad (4.14)$$

where '*' represents the convolution. As indicated in Fig. 4.1, $r(n)$ is passed to the filter bank demodulator h_p , $p = 0, 1, \dots, P-1$, and the output of each subchannel demodulation filter is downsampled by factor K . The received symbol for the subchannel p_1 at time frame n_1 can be expressed as:

$$y_{p_1}(n_1 + d) = \sum_{m=-\infty}^{\infty} r(m) h_{p_1}(n_1 K - m), \quad (4.15)$$

By substituting Eqs. (4.13), (4.14) into (4.15),

$$\begin{aligned} y_{p_1}(n_1 + d) &= \sum_{p=0}^{P-1} \sum_{n=-\infty}^{\infty} x_p(n) \sum_{m=-\infty}^{\infty} \sum_{k=-\infty}^{\infty} f_p(k - nK) c(m - k) h_{p_1}(n_1 K - m) \\ &+ \sum_{m=-\infty}^{\infty} e(m) h_{p_1}(n_1 K - m). \end{aligned} \quad (4.16)$$

Let $j = m - k$ and $l = k - nK$, Eq. (4.16) becomes

$$y_{p_1}(n_1 + d) = \sum_{p=0}^{P-1} \sum_{n=-\infty}^{\infty} x_p(n) \sum_{j=0}^{L_c-1} c(j) \sum_{l=0}^{L-1} f_p(l) h_{p_1}(n_1 - n) K - j - l) + \xi. \quad (4.17)$$

where ξ is defined in Eq. (4.10). By defining $\alpha_{pp_1}(n)$ and ζ as in Eqs. (4.12) and (4.11) respectively, Eq. (4.17) can be reduced to Eq. (4.8). **Formulation 1** is proven.

Remarks: When the filter bank based modulator/demodulator and the communication channel are all linear and time invariant, the term \bar{y}_{p_1} in Eq. (4.8) is deterministic for a given transmitted symbol $x_{p_1}(n_1)$. According to Eq. (4.9), \bar{y}_{p_1} is a weighted version of $x_{p_1}(n_1)$ and the weight $\alpha_{p_1 p_1}(n_1)$ is a constant for a given subchannel p_1 . Therefore in

general, the constellation points of $x_{p_1}(n_1)$ and \bar{y}_{p_1} are a one-to-one mapping. For each constellation point of $x_{p_1}(n_1)$, there is a corresponding constellation point \bar{y}_{p_1} which can be calculated by Eq. (4.9). All the possible values of \bar{y}_{p_1} form the set of constellation points at the receiving end of subchannel p_1 . The noise item ξ and interference item ζ are both random processes.

The following theorem derives a closed-form SER formula for MPSK modulation by calculating the PDF of $y_{p_1}(n_1 + d)$ and setting the detection boundaries for the optimal phase detector of each subchannel.

Theorem 1: When the transmitted symbols, $x_p(n)$, $0 \leq p \leq P - 1$, are coded by the MPSK scheme with symbol energy ϵ_x , and an optimal phase detector is adopted for each subchannel, the SER of the received symbol $y_{p_1}(n_1 + d)$, which corresponds to the transmitted symbol $x_{p_1}(n_1)$, can be determined as:

$$P_{e,p_1} = \frac{1}{\pi} \int_0^{\frac{(M-1)\pi}{M}} \exp \left[-\frac{\gamma \sin^2(\pi/M)}{\sin^2(\phi)} \right] d\phi, \quad (4.18)$$

where:

$$\gamma = \frac{|\alpha_{p_1 p_1}(n_1)|^2 \epsilon_x}{[\sum_{p,p \neq p_1} \sum_n |\alpha_{pp_1}(n)|^2 + \sum_{n,n \neq n_1} |\alpha_{p_1 p_1}(n)|^2] \epsilon_x + \sigma_n^2}, \quad (4.19)$$

is the signal to noise and interference ratio (SNIR), σ_n^2 is the variance of zero mean additive Gaussian random noise $e(n)$ and $\alpha_{pp_1}(n)$ is defined in Eq. (4.12).

Proof: In the MPSK coding scheme, the transmitted symbols $x_p(n)$ is coded as :

$$x_p(n) = \sqrt{\epsilon_x} e^{j\theta_k}, \quad k = 0, 1, \dots, M - 1, \quad (4.20)$$

where θ_k is the transmitted phase and takes one of the values from the set $\{(2\pi k)/M\}$. Due to the fact that the coefficients of modulator/demodulator and channel can be complex-valued, $y_{p_1}(n_1 + d)$ may be complex-valued as well. We denote the real and imaginary parts of $y_{p_1}(n_1 + d)$ as a and b .

To get the expression for the SER of $y_{p_1}(n_1 + d)$, the joint PDF $f_{AB}(a, b)$ must be formulated. In the following, we first derive the characteristic function of $y_{p_1}(n_1 + d)$.

Since $e(n)$ is a zero mean Gaussian random process, it is easy to see from Eq. (4.10) that ξ is a Gaussian random process with zero mean and variance

$$\sigma_{\xi}^2 = \sigma_n^2. \quad (4.21)$$

From Eq. (4.11), the interference ζ is the weighted sum of identical independent distributed (iid) random variables, $x_p(n)$, each with mean μ_x and variance σ_x^2 . According to the Central Limit Theorem [35], ζ approaches a Gaussian random process as the quantity of $x_p(n)$, which is mainly dominated by P , gets large. Moreover, the mean and variance of ζ can be calculated as:

$$\mu_{\zeta} = \sum_{p,p \neq p_1} \sum_n \alpha_{pp_1}(n) E[x_p(n)] + \sum_{n,n \neq n_1} \alpha_{p_1 p_1} E[x_{p_1}(n)], \quad (4.22)$$

$$\sigma_{\zeta}^2 = \sum_{p,p \neq p_1} \sum_n |\alpha_{pp_1}(n)|^2 Var[x_p(n)] + \sum_{n,n \neq n_1} |\alpha_{p_1 p_1}(n)|^2 Var[x_{p_1}(n)], \quad (4.23)$$

where $E[\cdot]$, $Var[\cdot]$ and $|\cdot|$ denote the expected value, the variance and the absolute value, respectively. Without loss of generality, assume

$$E[x_p(n)] = 0. \quad (4.24)$$

From Eq. (4.20),

$$Var[x_p(n)] = \epsilon_x, \quad (4.25)$$

for $p = 0, 1, \dots, P - 1$. Then the mean and variance of Gaussian random variable ζ can be obtained as:

$$\mu_{\zeta} = 0, \quad (4.26)$$

$$\sigma_{\zeta}^2 = \left[\sum_{p,p \neq p_1} \sum_n |\alpha_{pp_1}(n)|^2 + \sum_{n,n \neq n_1} |\alpha_{p_1 p_1}(n)|^2 \right] \epsilon_x, \quad (4.27)$$

Since the noise ξ and the interference ζ are independent to each other, the received symbol $y_{p_1}(n_1 + d)$ is a Gaussian random variable with mean \bar{y}_{p_1} and variance

$$\sigma_y^2 = \sigma_{\xi}^2 + \sigma_{\zeta}^2. \quad (4.28)$$

Using Eqs. (4.21) and (4.27), we get

$$\sigma_y^2 = \sigma_n^2 + \left[\sum_{p,p \neq p_1} \sum_n |\alpha_{pp_1}(n)|^2 + \sum_{n,n \neq n_1} |\alpha_{p_1 p_1}(n)|^2 \right] \epsilon_x. \quad (4.29)$$

The characteristic function of $y_{p_1}(n_1 + d)$ can be expressed as:

$$\Phi_y(v) = \exp(j\bar{y}_{p_1} v - \frac{v^2 \sigma_y^2}{2}). \quad (4.30)$$

The joint PDF of a and b can then be obtained with the characteristic function of $y_{p_1}(n_1 + d)$ as:

$$f_{AB}(a, b) = \frac{1}{2\pi\sigma_y^2} \exp \left[-\frac{[a - \text{Re}(\bar{y}_{p_1})]^2 + [b - \text{Im}(\bar{y}_{p_1})]^2}{2\sigma_y^2} \right]. \quad (4.31)$$

where $\text{Re}(\cdot)$ and $\text{Im}(\cdot)$ represent the real and imaginary parts of a complex-valued, respectively.

With the change of variables from (a, b) to (V, Θ_y) , which are defined as

$$V = \sqrt{a^2 + b^2}, \quad (4.32)$$

and

$$\Theta_y = \tan^{-1} \left(\frac{b}{a} \right), \quad (4.33)$$

the PDF of the detected phase Θ_y can be obtained by

$$f_{v\Theta}(V, \Theta_y) = \frac{V}{2\pi\sigma_y^2} \exp \left[-\frac{V^2 + |\bar{y}_{p_1}|^2 - 2V|\bar{y}_{p_1}| \cos(\Theta_y - \theta_{\bar{y}_{p_1}})}{2\sigma_y^2} \right], \quad (4.34)$$

where $\theta_{\bar{y}_{p_1}} = \tan^{-1} \left[\frac{\text{Im}(\bar{y}_{p_1})}{\text{Re}(\bar{y}_{p_1})} \right]$ is the phase of the output constellation point \bar{y}_{p_1} .

Since $y_{p_1}(n_1 + d)$ is a Gaussian random process, the optimal phase detector based on the maximum likelihood (ML) detection criterion can be employed to perform detection for subchannel p_1 . The operation principle of the optimal phase detector is to compute the phase of $y_{p_1}(n_1 + d)$ and select the constellation point, from the constellation set of \bar{y}_{p_1} , with the smallest phase difference relative to $y_{p_1}(n_1 + d)$. Then the transmitted symbol is determined from the one-to-one mapping relation between the constellation points of $x_{p_1}(n_1)$ and \bar{y}_{p_1} . The decision boundaries for $y_{p_1}(n_1 + d)$ can be determined based on the

constellation points of \bar{y}_{p_1} . According to Eq. (4.9), \bar{y}_{p_1} is a scaled version of $x_{p_1}(n_1)$ and the weight $\alpha_{p_1}(n_1)$ is a constant for a given subchannel, i.e. the phase difference between the constellation points of \bar{y}_{p_1} is same as that of transmitted symbol $x_{p_1}(n_1)$. Therefore the phase difference of any two adjacent constellation points of \bar{y}_{p_1} is $2\pi/M$. Without loss of generality, we assume the phase of the transmitted symbol $x_{p_1}(n_1)$ is 0. In this case, no decision error will happen if the phase of $y_{p_1}(n_1 + d)$ falls inside the range Λ , which is denoted as

$$\Lambda = \left[-\frac{\pi}{M} + \theta_{\bar{y}_{p_1}}, \frac{\pi}{M} + \theta_{\bar{y}_{p_1}} \right], \quad (4.35)$$

To calculate the SER, the integration range of the variable V in Eq. (4.34) is $[0, +\infty)$, which is computationally complex. In the following, we convert the integration over the infinite range into a integration over a finite range. The variable (V, Θ_y) in Eq. (4.34) are replaced with (r, ψ_y) , which are defined as follows:

$$r = \sqrt{V^2 + 2V \cos(\Theta_y - \theta_{\bar{y}_{p_1}}) |\bar{y}_{p_1}| + |\bar{y}_{p_1}|^2}, \quad (4.36)$$

$$\psi_y = \tan^{-1} \left[\frac{V \sin(\Theta_y - \theta_{\bar{y}_{p_1}})}{V \cos(\Theta_y - \theta_{\bar{y}_{p_1}}) + |\bar{y}_{p_1}|} \right], \quad (4.37)$$

Then the PDF of (r, ψ_y) is

$$f_{r\psi_y}(r, \psi_y) = \frac{r}{2\pi\sigma_y^2} \exp\left(-\frac{r^2}{2\sigma_y^2}\right). \quad (4.38)$$

Please refer to the Appendix B for the details of Eqs. (4.36)-(4.38). According to [36, 37, 38, 39], the SER can be calculated as

$$P_{e,p_1} = 2 \int_0^{\frac{(M-1)\pi}{M}} d\psi \int_R^\infty f_{r\psi_y}(r, \psi_y) dr, \quad (4.39)$$

where $R = \frac{|\bar{y}_{p_1}| \sin(\pi/M)}{\sin(\psi_y + \pi/M)}$, and the expression of SER can be simplified as in Eq. (4.18), where

$$\gamma = \frac{|\bar{y}_{p_1}|^2}{\sigma_y^2}. \quad (4.40)$$

By substituting Eqs. (4.9) and (4.29) into Eq. (4.40), we get Eq. (4.19). Thus **Theorem 1** is proved.

The overall SER for a MPSK-OFDM system, P_e , can be obtained by averaging P_{e,p_1} over all P subchannels,

$$P_e = \frac{1}{P} \sum_{p_1=0}^{P-1} P_{e,p_1}. \quad (4.41)$$

4.1.3 SER Expression for AWGN Channels

For an AWGN channel or a channel which is perfectly equalized, expression of SER for a generic MPSK-OFDM system can be simplified on the basis of Eq. (4.19). For an AWGN channel, $c(n) = \delta(n)$. It can be seen from Eq. (4.2) that

$$\alpha_{pp_1}(n) = \begin{cases} 1 & p = p_1 \text{ and } n = n_1, \\ 0 & \text{otherwise,} \end{cases} \quad (4.42)$$

i.e., the only symbol which has nonzero contribution to $y_{p_1}(n_1 + d)$ is $x_{p_1}(n_1)$. Since $\sigma_y^2 = \sigma_n^2$, the SNIR γ in Eq. (4.19) becomes

$$\gamma = \rho = \frac{\epsilon_x}{\sigma_n^2}, \quad (4.43)$$

which is the signal-to-noise ratio (SNR). From Eq. (4.41) the overall SER, P_e is

$$P_e = P_{e,p_1}. \quad (4.44)$$

By substituting Eq. (4.42) into Eq. (4.18), we get the SER for a MPSK-OFDM system, which is identical to the SER formula for a single carrier MPSK system over AWGN channels. With the increase of SNR, the SER will decrease quickly. It can also be seen from Eq. (4.44) that for an AWGN channel, the number of subchannels, P , has no effect on the system error performance. Fig. 4.2 shows the SER results for both single carrier modulation and the conventional DWT modulation, with different numbers of subchannels, over an AWGN channel. The modulation scheme adopted is binary phase shift keying (BPSK).

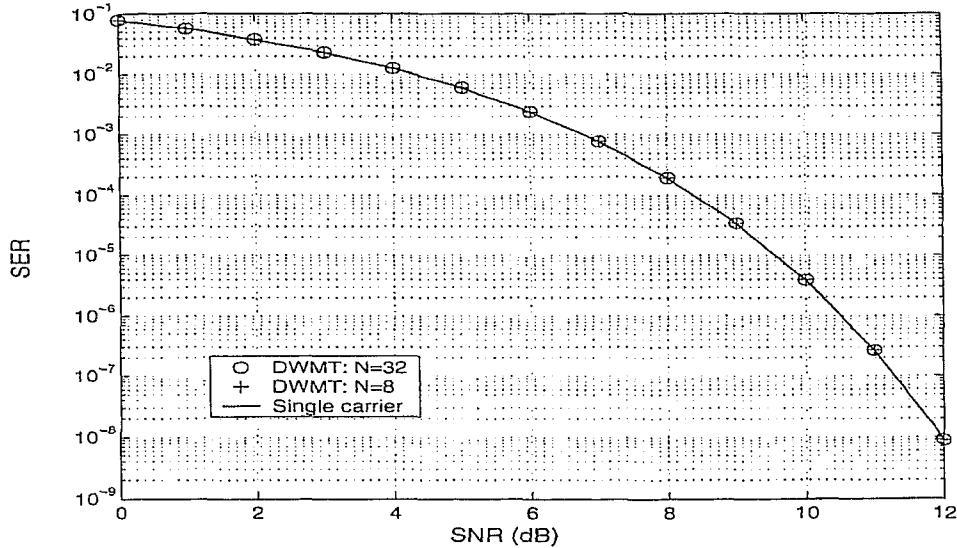


Figure 4.2: Error performance of single carrier modulation and the conventional DWMT ($g = 2$) modulation with BPSK

4.1.4 SER Expression for Fading Channels

To investigate the performance of OFDM systems over fading channels, we rewrite γ in Eq. (4.19) in an alternative expression as

$$\gamma = \frac{|\alpha_{p_1 p_1}(n_1)|^2 \rho}{[\sum_{p,p \neq p_1} \sum_n |\alpha_{pp_1}(n)|^2 + \sum_{n,n \neq n_1} |\alpha_{p_1 p_1}(n)|^2] \rho + 1}. \quad (4.45)$$

It can be seen from Eq. (4.45) that when SNR ρ is much larger than 1 (0dB), P_{e,p_1} is dominated by the ratio of weights for the desired symbol and the interference, which can be approximated as

$$\gamma \approx \frac{|\alpha_{p_1 p_1}(n_1)|^2}{\sum_{p,p \neq p_1} \sum_n |\alpha_{pp_1}(n)|^2 + \sum_{n,n \neq n_1} |\alpha_{p_1 p_1}(n)|^2}. \quad (4.46)$$

In this case, the SER performance will not change much with the increase of SNR ρ . Fig. 4.3 shows the error performance of a DWMT system, with overlapping factor $g = 2$, over a sample fading channel.

For DFT-based OFDM systems, from Eq. (4.12), the inclusion of zero-padded CP does not change the value of numerator in Eq. (4.46), but the value of the denominator will decrease because of the increase of the upsampling/downsampling factor K . Therefore,

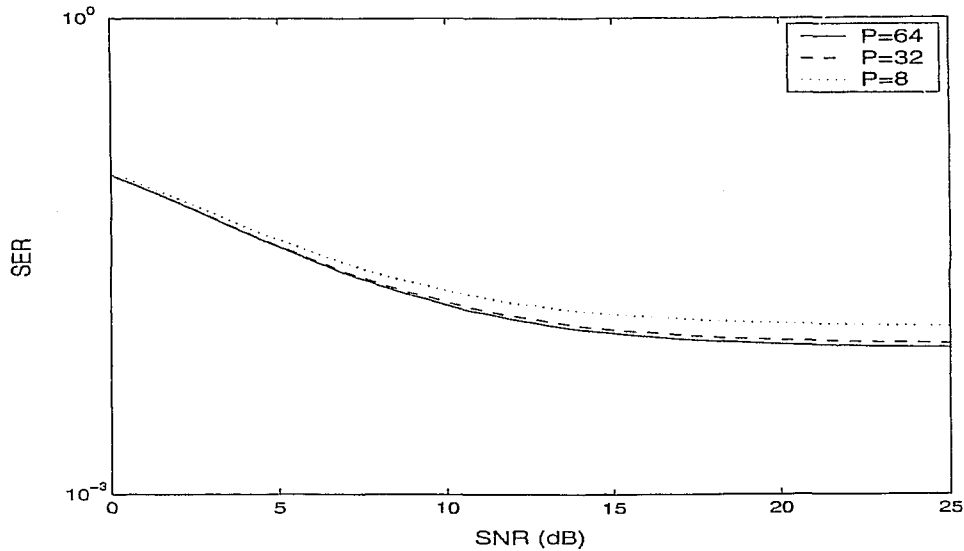


Figure 4.3: Error performance of the conventional DWMT systems ($g = 2$) over channel $c(n) = [1, 0.5e^{j\pi/6}, 0.3e^{-j\pi/3}, 0.2e^{j\pi/2}, 0.1]$.

DFT-based OFDM systems with CP will demonstrate superior error performance than DFT-based OFDM systems without CP.

Expressions of (4.18) and (4.41) provide a systematic approach to calculate the SER of a generic MPSK-OFDM system, which fulfills the orthogonality and PR conditions in Eqs. (4.1) and (4.2). Moreover, the SER formula can be used as the objective function in the design of modulation and demodulation filter banks for an OFDM system to achieve better error performance. In the following, a novel OFDM system, based on complex-valued unitary filter banks designed to minimize SER, is presented.

4.2 Complex-Valued Unitary Filter Bank Based OFDM System Design

Unitary filter banks are a special class of maximally decimated ($P = K$) PR filter banks. A unitary filter bank is a good candidate to the modulator/demodulator for an OFDM system because the inherent mutual orthogonality among its filters. Unitary filter banks with FIR filters have many useful properties. Among these properties are that they

can be completely factorized, are easy to implement with a lattice structure and have no questions of stability [26]. Moreover, they can be used to construct orthonormal multiband wavelet bases, which are powerful tools for non-stationary signal analysis. Due to the existence of complex-valued signals in wireless systems, complex-valued filters, which have asymmetric frequency responses, are proposed in this paper. The complex-valued filter bank is completely parameterized and the coefficients of all filters are expressed with free parameters, which can be determined on basis of different applications. In this paper, the SER, expressed in (4.18) and (4.41) of an OFDM system which employs MPSK coding scheme for all P subchannels, is taken as the objective function to optimize the performance of the designed filter banks.

4.2.1 Parameterization of Filter Bank Coefficients

The Householder factorization of the polyphase component matrices of modulation filters $\{f_0, f_1, \dots, f_{P-1}\}$ can be summarized as follows [26, 40]. The z -transform of filter f_p , $p = 0, 1, \dots, P - 1$ can be formulated in the polyphase form as:

$$\mathbf{F}_p(z) = \sum_{k=0}^{P-1} z^{-k} \mathbf{F}_{p,k}(z^P). \quad (4.47)$$

Define the polyphase component matrices $\mathbf{F}(z)$ as follows:

$$(\mathbf{F}(z))_{p,k} = \mathbf{F}_{p,k}(z). \quad (4.48)$$

If $\mathbf{F}(z)$ is a unitary matrix, i.e.

$$\mathbf{F}^T(z^{-1})\mathbf{F}(z) = \mathbf{I}, \quad (4.49)$$

where \mathbf{I} is the identity matrix, then $\mathbf{F}(z)$ has the Householder factorization

$$\mathbf{F}(z) = \left\{ \prod_{n=1}^{J-1} [\mathbf{I} - \mathbf{v}_n \mathbf{v}_n^H + z^{-1} \mathbf{v}_n \mathbf{v}_n^H] \right\} \mathbf{V}, \quad (4.50)$$

where J is the McMillan degree of $\mathbf{F}(z)$, \mathbf{v}_n is unit-norm Householder parameters, and \mathbf{V} is a $P \times P$ constant unitary matrix which can be selected according to various applications. As a special case, for filter banks associated with P band wavelet transforms,

the unitary matrix \mathbf{V} may be generated by assigning one column as a constant vector $[\frac{1}{\sqrt{P}}, \frac{1}{\sqrt{P}}, \dots, \frac{1}{\sqrt{P}}]^T$ which corresponds to the scaling filter, then adding orthogonal columns to generate wavelet filter vectors [41], [42]. The $P-1$ orthogonal columns may be produced via the Gram-Schmidt process in $\binom{P-1}{2}$ ways.

The Householder parameters are of unit norm, therefore each Householder parameter in Eq. (4.50) can be further parameterized as [40]:

$$\mathbf{v}_{n,j} = \begin{cases} \left[\prod_{k=0}^{j-1} \sin(\theta_{n,k}) \right] \cos(\theta_{n,j}) e^{j\phi_{n,j}}, & j = 0, 1, \dots, P-2 \\ \prod_{k=0}^{P-2} \sin(\theta_{n,k}), & j = P-1, \end{cases} \quad (4.51)$$

for $n = 1, \dots, J-1$, i.e., $\mathbf{v}_{n,j}$ can be determined by $2(P-1)$ angle parameters. After \mathbf{V} has been determined, the filter bank $\{f_0, f_1, \dots, f_{P-1}\}$ is determined by $2(J-1)(P-1)$ angle parameters. The length of filters f_p , $p = 0, 1, \dots, P-1$, is $L = JP$.

The relation between modulation filters and demodulation filters can be expressed as

$$h_p(l) = f_p^*(-l), \quad (4.52)$$

where $p = 0, 1, \dots, P-1$ and $l = -L+1, -L+2, \dots, 0$.

4.2.2 SER Improvement Based on Proposed Filter Banks

To calculate all filter coefficients in Eq. (4.50), the constant matrix \mathbf{V} and the free parameters $\theta_{n,k}$, $\phi_{n,j}$, in Eq. (4.51) should all be determined. The procedure to design an OFDM system based on the P -band complex-valued unitary filter bank to optimize SER performance is outlined as follows.

- Step 1: Choose the unitary matrix \mathbf{V} according to different applications. For simplicity, we propose \mathbf{V} as the $P \times P$ DFT matrix, which is defined as

$$\mathbf{V}_{nk} = \sqrt{\frac{1}{P-1}} e^{-j2\pi(k-1)(n-1)}, \quad (4.53)$$

for $k, n = 1, 2, \dots, P$.

- Step 2: Define the objective function. We take the SER formula for a MPSK coded OFDM system expressed in Eq. (4.41), which is reproduced in the following, as the objective function:

$$P_e = \frac{1}{P} \sum_{p_1=0}^{P-1} P_{e,p_1}, \quad (4.54)$$

where P_{e,p_1} can be calculated by

$$P_{e,p_1} = \frac{1}{\pi} \int_0^{\frac{(M-1)\pi}{M}} \exp \left[-\frac{\gamma \sin^2(\pi/M)}{\sin^2(\phi)} \right] d\phi, \quad (4.55)$$

where γ is a function of coefficients of modulation/demodulation filters, which in turn are functions of free parameters $\theta_{n,j}$ and $\phi_{n,j}$, $j = 1, 2, \dots, P-2$, $n = 0, 1, \dots, J-1$.

- Step 3: Apply a numerical optimization methods to determine the values of free parameters. First set up initial values for all free parameters $\theta_{n,j}$ and $\phi_{n,j}$, $j = 0, 1, \dots, P-2$, $n = 1, 2, \dots, J-1$, then a conjugate gradient method can be used to minimize the $2(J-1)(P-1)$ dimensional function P_e . Note that the optimization may fall into a local minimum. Some global optimization methods such as adding random interference and simulated annealing may also be used. However, in practice, a local minimum may be satisfactory as well.

4.3 Simulations

To verify our theoretical analysis of error performance of a generic MPSK-OFDM system, Monte-Carlo numerical simulations are performed with three types of OFDM systems, namely the DFT-based OFDM system with zero-padded CP which is no shorter than the length of the transmission channel, the DFT-based OFDM without CP, and the conventional DWMT systems with overlapping factor $g = 2$, whose modulation filters are generated by prototype filter [32]

$$w(l) = \sin \left[\frac{\pi}{2P} \left(l + \frac{1}{2} \right) \right]. \quad (4.56)$$

for $l = 0, 1, 2P - 1$. Both AWGN channels and fading channels are considered in the simulations. In simulations, the procedure to calculate the SER for a specific SNR is outlined in the flowchart of Fig. 4.4. The quantity of symbols generated in simulations is 10^6 .

In system simulation, the transmitted MPSK data streams $x_p(n)$, $p = 0, 1, \dots, P - 1$, are generated according to Eq. (4.20). The composite data sequence before the channel, $s(n)$, as illustrated in Fig. 4.1, are obtained by first upsampling each of the MPSK symbol stream $\{x_0(n), x_1(n), \dots, x_{P-1}(n)\}$ by factor K , then convolving each data stream with one of the P subchannel modulation filters, finally summing up the outputs of all P modulation filters. After $s(n)$'s convolution with the channel $c(n)$, the AWGN noise, whose power is calculated according to a particular SNR, is added to the transmitted sequence to obtain distorted data sequence $r(n)$. Then $r(n)$ is passed through the demodulation filter of each subchannel, and the result signals are downsampled by factor K . An optimal phase detector is employed for each subchannel according to the preset phase detection boundaries. Matching of the detected symbol with the original data is made and errors are counted to obtain SER for the particular SNR.

Fig. 4.5 and 4.6 show both the analytical and simulation results over an AWGN channel for DFT-based OFDM systems with and without zero-padded CP, and DWMT generated with prototype filter expressed in Eq. (4.56). The modulation scheme is quadrature phase shift keying (QPSK) and the number of subchannels are 16 and 32, respectively. It can be seen that our theoretical analysis matches the simulations results. In addition, all three kinds of OFDM systems exhibit the same error performance as that in single-carrier systems over an AWGN channel and this performance does not change with the number of subchannels. The identical SER performance of single carrier systems and OFDM systems over AWGN channels has been explained in section 4.1.3.

Figs. 4.8 and 4.9 show the results of these OFDM systems, with $P = 16$ subchannels, over two sample multipath fading channels with impulse response $c_1(n) = [1, 0.5e^{j\pi/6}]$ and $c_2(n) = [1, 0.5e^{j\pi/6}, 0.3e^{-j\pi/3}, 0.2e^{j\pi/2}, 0.1]$ for QPSK symbols, respectively. The am-

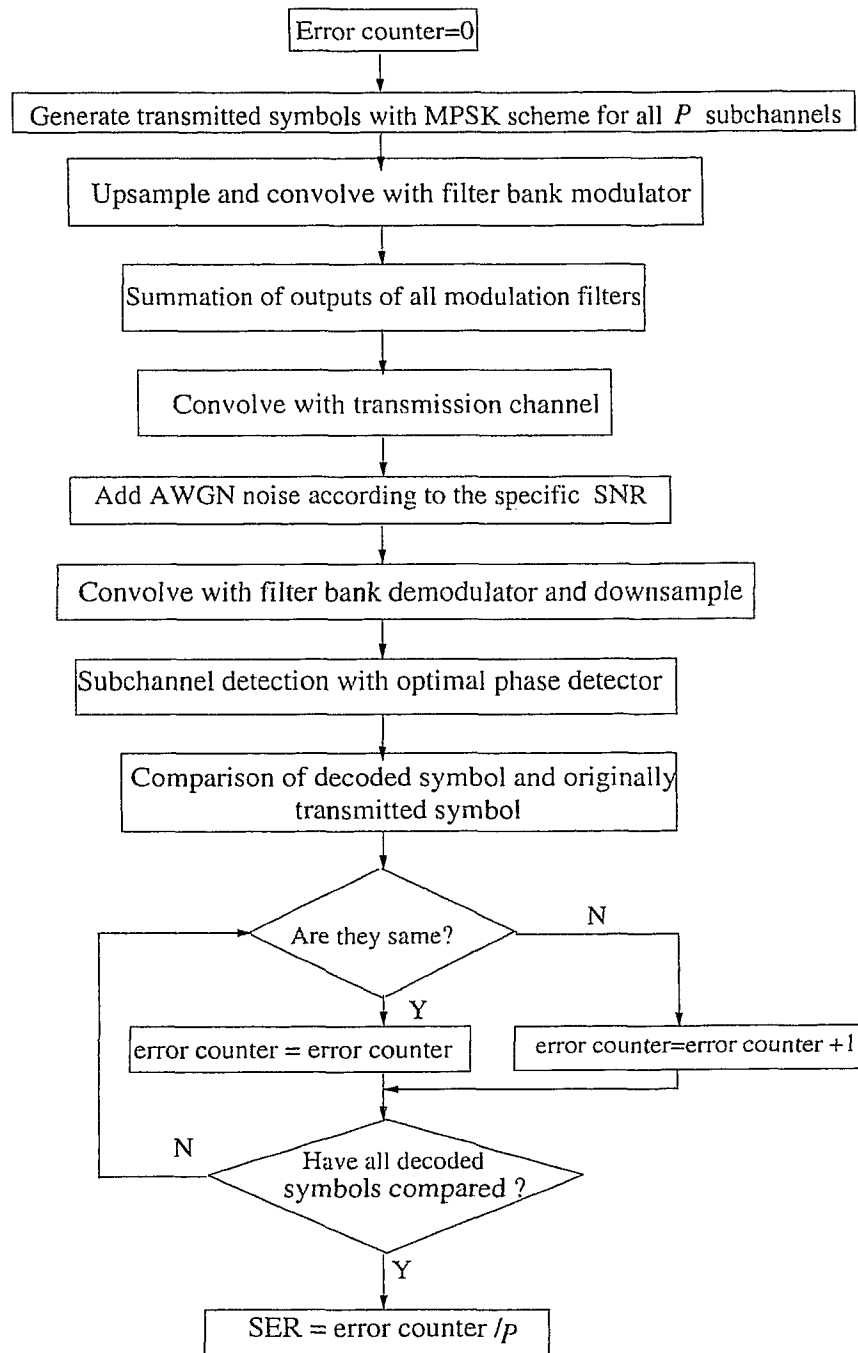


Figure 4.4: Flowchart of system simulation

plitude characteristics of frequency responses of both channels are shown in Fig. 4.7. Fig. 4.10 and 4.11 show the results of these OFDM systems, with $P = 32$ subchannels,

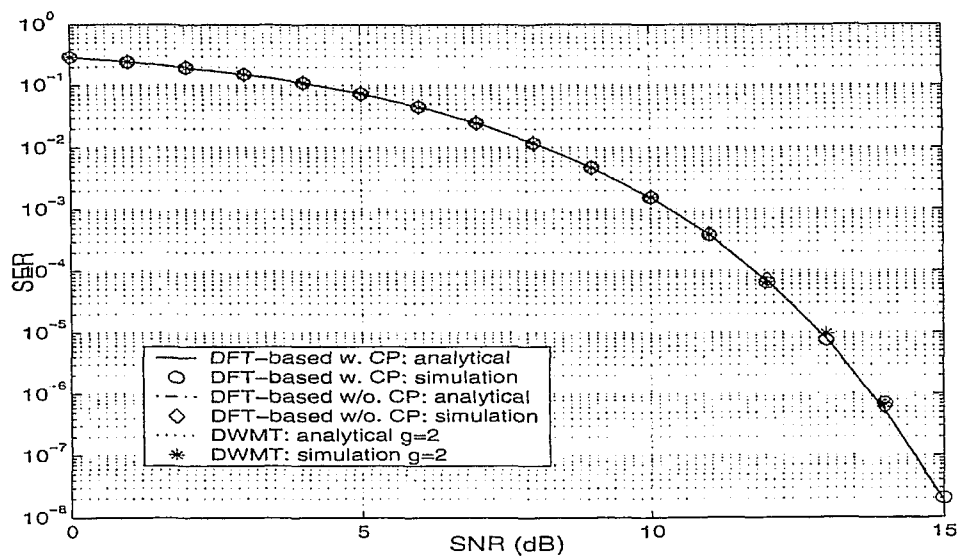


Figure 4.5: Comparison of the analytical and simulated performance of OFDM systems over AWGN channels: QPSK ($P = 16$)

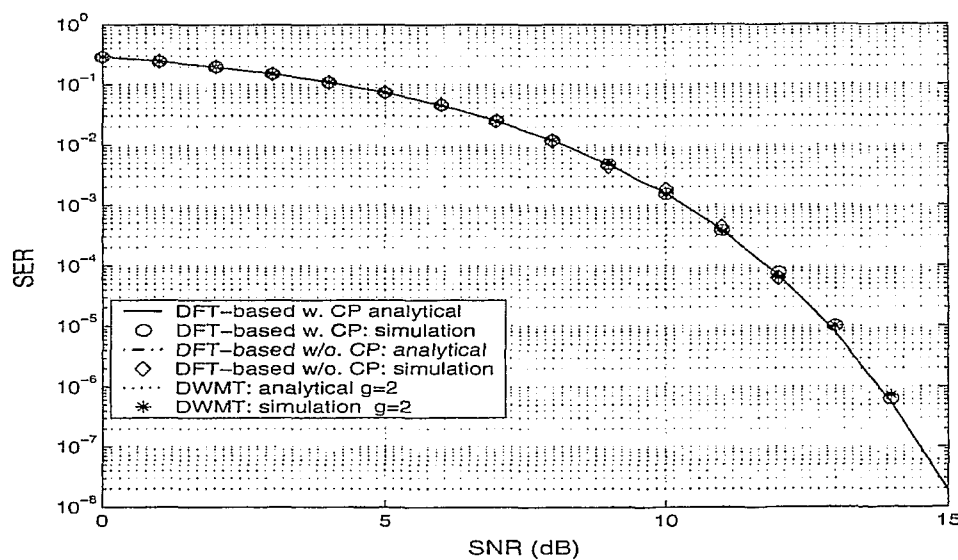


Figure 4.6: Comparison of the analytical and simulated performance of OFDM systems over AWGN channels: QPSK ($P = 32$)

over the two sample multipath fading channels $c_1(n)$ and $c_2(n)$ for QPSK symbols. Each simulation result demonstrates the consistency with corresponding theoretical analysis. As expected, the DFT-based OFDM system with CP has superior SER over the other

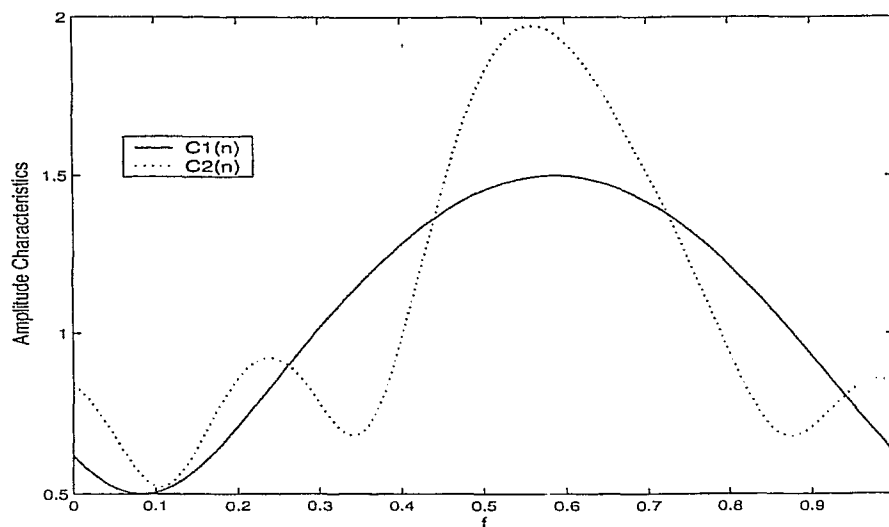


Figure 4.7: Amplitude characteristics of frequency responses of two channels used in simulations

two OFDM systems, with the cost of system efficiency. It is also demonstrated that the DWMT has the poorest SER. The reason is that both channels have no narrow band interference in comparison to the bandwidth of the subchannels. Therefore, ISI is the dominant effect on the SER than ICI, which DWMT is designed to minimize. Moreover, since the filters in DWMT are of longer length, the dispersive channel may distort more symbols and increase ISI.

To investigate the error performance of the new OFDM based on filter banks designed in section 4.2, simulations are performed with a DFT-based OFDM with zero-padded CP, a conventional DWMT system of which the prototype filter is defined in Eq. (4.56), and the new OFDM system based on complex-valued unitary filter banks. The filters of both the DWMT system and the new OFDM system are of length $L = 2P$. As shown in Figs. 4.12 and 4.13, that the new OFDM system based on proposed complex-valued unitary filter banks has better SER than the DWMT system. Its performance is comparable to that of the CP included DFT-based OFDM, whose transmission efficiency is decreased by a factor of $\frac{P}{P+L_k}$, where L_k is the length of CP. L_k is chosen no less than the length of

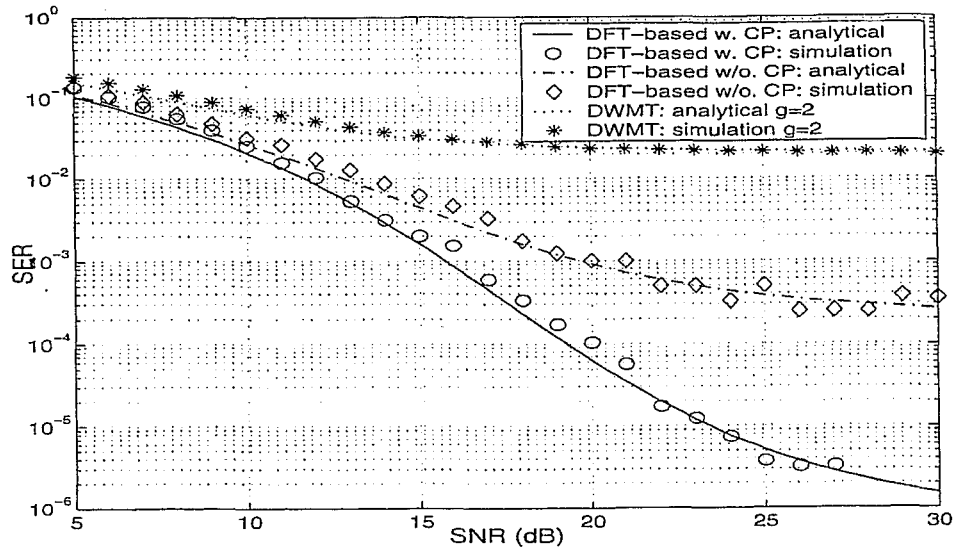


Figure 4.8: Comparison of the analytical and simulated performance of OFDM systems with QPSK coding over channel $c_1(n)$ ($P = 16$)

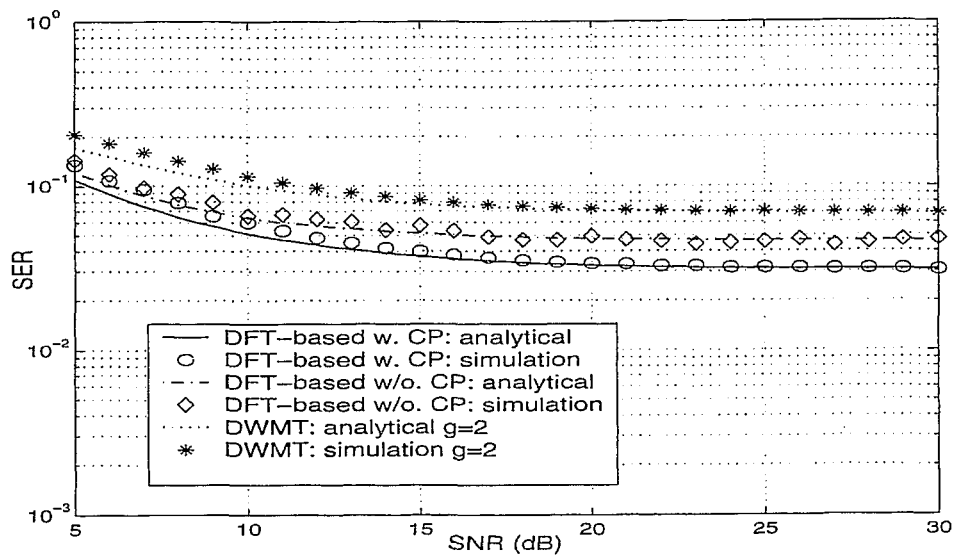


Figure 4.9: Comparison of the analytical and simulated performance of OFDM systems with QPSK coding over channel $c_2(n)$ ($P = 16$).

channel.

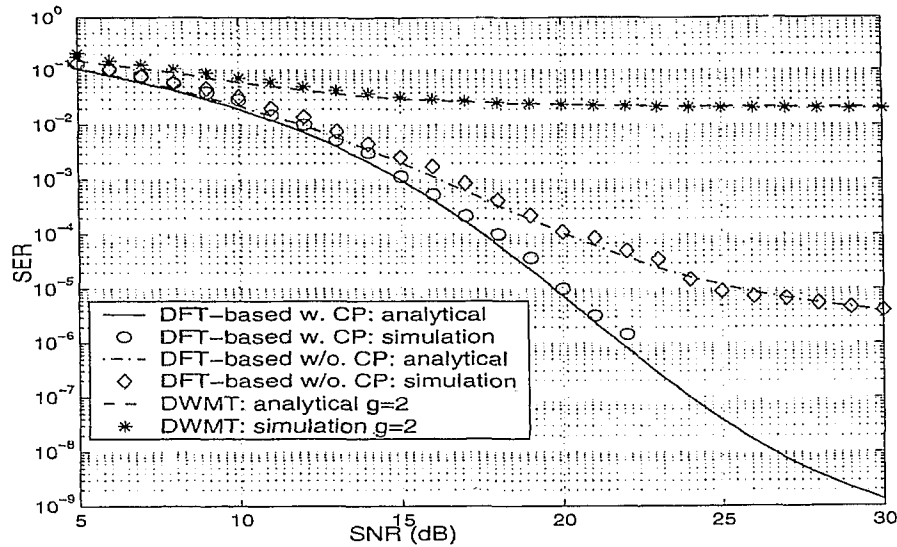


Figure 4.10: Comparison of the analytical and simulated performance of OFDM systems with QPSK coding over channel $c_1(n)$ ($P = 32$)

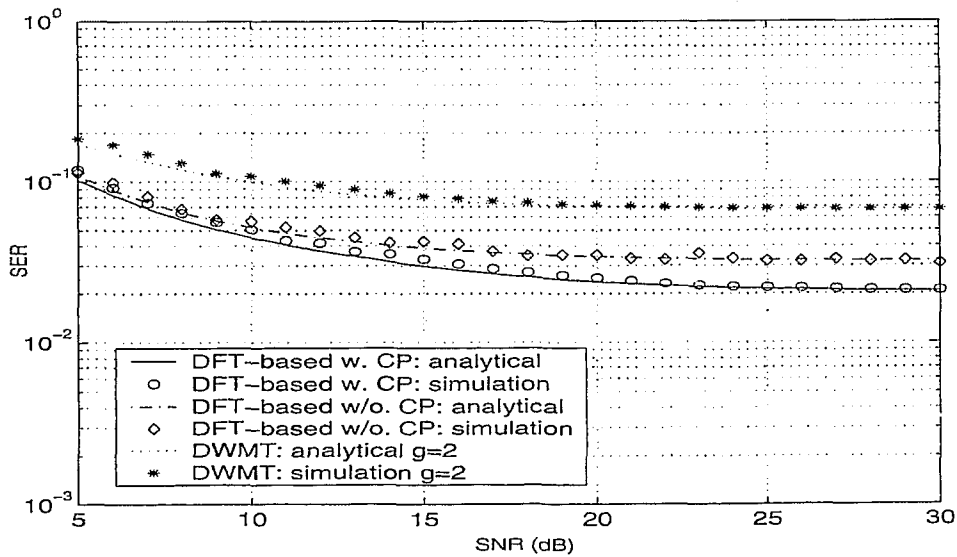


Figure 4.11: Comparison of the analytical and simulated performance of OFDM systems with QPSK coding over channel $c_2(n)$ ($P = 32$).

4.4 Summary

In this chapter, a closed-form formula of SER is derived for a generic OFDM system with MPSK modulation and optimum phase detection in each subchannel, based on the

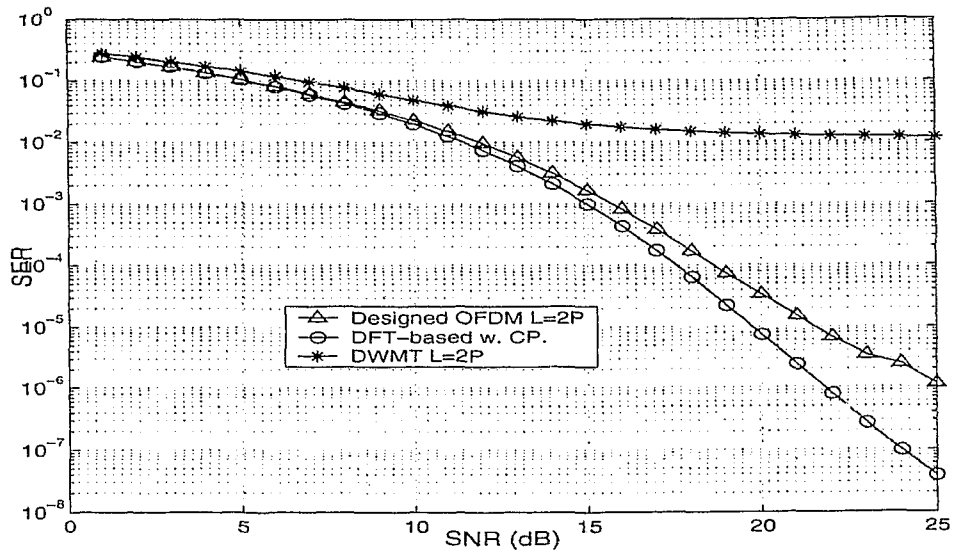


Figure 4.12: System performance of different OFDM systems with QPSK modulation over channel $c_1(n)$ ($P = 32$).

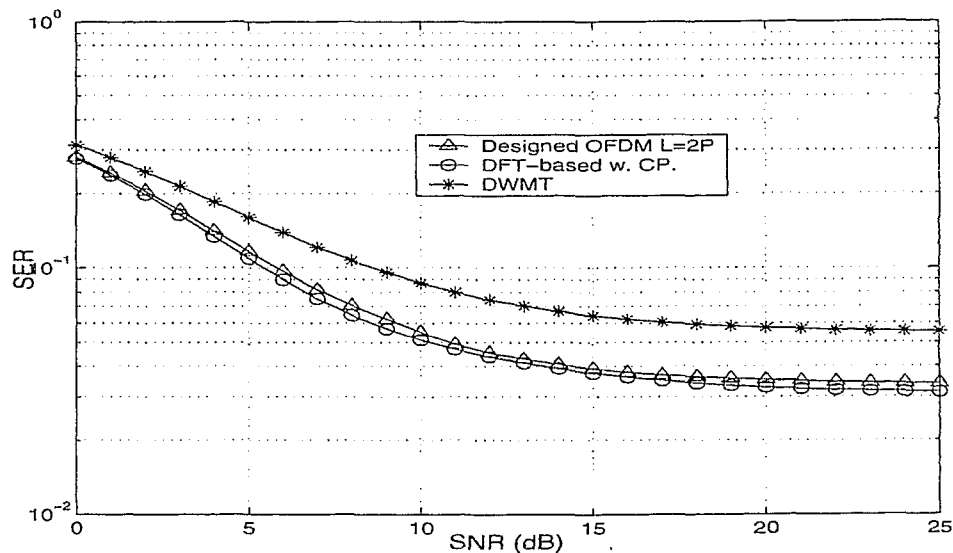


Figure 4.13: System performance of different OFDM systems with QPSK modulation over channel $c_2(n)$ ($P = 32$).

constellation points of received symbols and the assumption that the sum of ISI and ICI can be modelled as a Gaussian random processes. It is shown that for AWGN channels, OFDM systems demonstrate identical SER performance with single carrier systems. For

fading channels, when SNR is far bigger than 0dB, SER of an OFDM will be dominated by the ratio of weights for desired symbol and interference. This formula can be used to evaluate DFT-based OFDM and DWMT systems as well as to design new OFDM systems.

By employing the derived formula as the objective function, we present a design method for a novel OFDM system based on complex-valued multiband unitary filter banks to minimize SER. The proposed OFDM system has more flexible frequency response and is more suitable to deal with complex-valued signals present in wireless systems. This design method provides flexibility in choosing OFDM subchannels for different applications by optimizing filter banks towards different objective functions.

Simulations are performed with DFT-based OFDM systems with and without zero-padded CP, and the DWMT system with overlapping factor $g = 2$. Simulation results show the consistency of theoretical SER analysis and numerical simulations. Moreover, simulations demonstrated that the designed OFDM system outperforms the conventional DWMT systems, filters of both systems are of same length, in terms of SER, the performance of the designed OFDM is also comparable to that of the DFT-based OFDM with zero-padded CP, while the latter system compromises transmission efficiency for better error performance.

Chapter 5

Joint Maximum Likelihood Detection Algorithm for OFDM Systems and Error Performance Analysis

IN Chapter 4, the error performance of a generic OFDM system is investigated by considering transmitted symbols of each subchannel individually. When detecting the received symbols of a given subchannel, all transmitted symbols on the other subchannels are considered as random ICI interference. We refer this detection algorithm as the subchannel algorithm which has been adopted in many attempts recently [6, 17, 18, 19, 20, 21] when evaluating the error performance of an OFDM system. However, when employing the subchannel detection algorithm, the detection and decoding of a given subchannel does not take advantage of the information carried by the other subchannels to obtain a better evaluation of the transmitted symbols of the given subchannel, and to improve the system error performance.

In this chapter, a joint detection algorithm is proposed for a generic OFDM system to jointly detect and decode symbols received in one frame. The main advantage of the joint detection algorithm is that it turns the mutual effects, of subchannel symbols to be jointly decoded, from interference into useful information contributing to the constellation points of each other.

As explained in Section 3.1.1, in a P -subchannel OFDM system, during each time frame, P symbols, with each one modulated to one of P subchannels, are transmitted in parallel. The transmitted symbols are modulated with discrete schemes, such as MPSK and quadrature amplitude modulation (QAM). For a given frame, the transmitted symbol of a given subchannel is a one-dimensional symbol. The alphabet size of the constellation points, for the one-dimensional transmitted symbol, is finite. As a result, the alphabet size of the constellation points of the P -dimensional transmitted symbol, which consists of symbols transmitted on all P subchannels at the given frame, is also finite. The transmitted P -dimensional symbol and received P -dimensional symbol are referred as the transmitted OFDM symbol and received OFDM symbol respectively. For the case that the filter bank modulator and demodulator and the transmission channel are all linear and time invariant, all the constellation points of a received OFDM symbol can be obtained.

Considering the alphabet size of the constellation points of a received OFDM symbol will increase exponentially with the increase of the number of subchannels, P , the received OFDM symbol is evenly partitioned into a number of subsets, which consisting symbols with lower dimensions, to prohibit excessive computation load. The subchannel symbols received in one subset, referred as a received vector symbol, are jointly detected by considering the effects of all subchannels excluded in the subset as interference. In this way, the ICI involved in a received symbol is partially reduced.

In this chapter, for linear and time invariant filter bank modulator/demodulator and transmission channels, the constellation points and the PDF of the received vector symbol are derived. The maximum likelihood (ML) criterion is employed to decode a received vector symbol by comparing the Mahalanobis distances between the received vector symbol and each of the constellation points of the received vector symbol, and decode the received vector symbol as the constellation point which is the closest to the receive vector symbol in terms of the Mahalanobis distance. A lower bound and an upper bound of the vector symbol error rate (VSER) are derived to provide a practical viewpoint of the system error performance by employing the proposed joint detection algorithm. Sim-

ulations are performed to investigate the performance of the joint detection algorithm. Simulation results show that the joint detection algorithm has superior error performance to subchannel detection algorithm.

This chapter is outlined as follows. In Section 5.1, the joint detection algorithm for a generic OFDM system is presented by deriving the constellation points of the received vector symbols in 5.1.2, then investigating the PDF of received vector symbols and ML detection in 5.1.3, and finally analyzing the system error performance under joint ML algorithm, and deriving a lower and an upper bounds of the VSER in 5.1.4. Results of numerical simulations are demonstrated in Section 5.2. Section 5.3 concludes the chapter.

5.1 Joint Detection Algorithm for OFDM Systems

5.1.1 System Modelling

A generic block diagram of an OFDM filter bank modulator and demodulator with P subchannels is shown in Fig. 4.1, which is reproduced below.

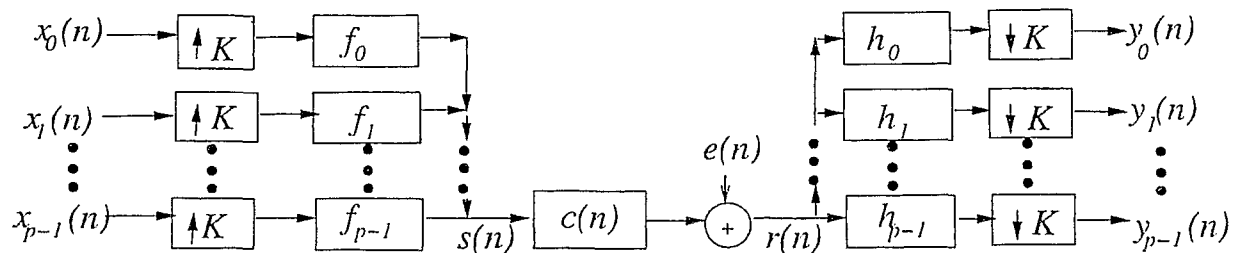


Figure 5.1: Block diagram for filter bank modulator and demodulator in OFDM systems

The theoretical model of a generic OFDM system is the same as in section 4.1.1, and it is reiterated here. The upsampling/downsampling factor $K = P + L_k$ for DFT-based OFDM systems, where L_k is the length of zero-padded CP, and $K = P$ for DWMT and other OFDM systems without CP [13]. Modulation and demodulation filters of the subchannel p are respectively denoted as f_p and h_p , $p = 0, 1, \dots, P - 1$. Both filters are of length $L = gK$, where g is the overlapping factor, $g = 1$ for DFT-based OFDM and $g \geq 2$ for DWMT systems. The constraint for the set of modulation filters is that, f_p ,

$0 \leq p \leq P - 1$, fulfill the following orthogonality property,

$$\sum_{l=0}^{L-1} f_{p_1}(l) f_{p_2}^*(l - nK) = \delta(n) \delta(p_1 - p_2), \quad 0 \leq p_1, p_2 \leq P - 1. \quad (5.1)$$

Moreover, the modulation and demodulation filters satisfy the PR property defined as

$$\sum_{l=0}^{L-1} f_{p_1}(l) h_{p_2}(nK - l) = \delta(n) \delta(p_1 - p_2), \quad 0 \leq p_1, p_2 \leq P - 1. \quad (5.2)$$

The transmission channel $c(n)$ is modelled as a LTI FIR filter of length L_c , followed by a stationary zero-mean Gaussian random noise source $e(n)$, which is independent of transmitting symbols $\{x_p(n), p = 0, 1, \dots, P - 1\}$. $c(n)$ is the overall transfer function resulting from the real communication channel and a time domain equalizer if there is a one. The mapping schemes for transmitted symbols are discrete, such as MPSK and PAM.

5.1.2 Constellation Points of Received Vector Symbols

For a P -subchannel OFDM system, during each time frame, a P -dimensional OFDM symbol, which consists of P parallel symbols $\{x_0(n), x_1(n), \dots, x_{P-1}(n)\}$, is transmitted. This OFDM symbol can be partitioned into P/J subsets, each of size J to form P/J J -dimensional vector symbols, if P is an integer multiple of J . Without loss of generality, the subset consisting of subchannels with index $\{p_1, p_1 + 1, \dots, p_1 + J - 1\}$, is taken as an example for following analysis. The subchannels indices in subset p_1 is denoted as subset p_1 . The group of indexes of subchannels in subset p_1 is expressed as $\mathcal{P}(p_1) = \{p_1, p_1 + 1, \dots, p_1 + J - 1\}$. The symbols of subset p_1 at a given frame n_1 are defined with the J -dimensional column vector, $\mathbf{X}_{p_1}(n_1)$,

$$\mathbf{X}_{p_1}(n_1) = [x_{p_1}(n_1), x_{p_1+1}(n_1), \dots, x_{p_1+J-1}(n_1)]^T. \quad (5.3)$$

All elements of $\mathbf{X}_{p_1}(n_1)$ are modulated with discrete mapping schemes, therefore the number of values which $\mathbf{X}_{p_1}(n_1)$ can take, or the cardinality of the alphabet set of $\mathbf{X}_{p_1}(n_1)$, represented with G , is finite. This cardinality can be determined by the mapping schemes

of all subchannels in the subset. If the cardinality of the alphabet set for the subchannel p , $p \in \mathcal{P}(p_1)$, is M_p , the alphabet size of $\mathbf{X}_{p_1}(n_1)$ will consist of $\prod_{p,p \in \mathcal{P}} M_p$ elements because all subchannels are coded independently. As a special case, if all subchannels in the subset p_1 are coded with the same M -ary coding scheme, then the cardinality of the alphabet set of $\mathbf{X}_{p_1}(n_1)$ is M^J . The set of all values that $\mathbf{X}_{p_1}(n_1)$ can take is denoted as the constellation set C_X . Corresponding to the transmitted vector symbol at frame n_1 , $\mathbf{X}_{p_1}(n_1)$, the received vector symbol is denoted as

$$\mathbf{Y}_{p_1}(n_1 + d) = [y_{p_1}(n_1 + d), y_{p_1+1}(n_1 + d), \dots, y_{p_1+J-1}(n_1 + d)]^T, \quad (5.4)$$

where d is the system delay involved in the convolution with modulation filters and demodulation filters, and other operations in the transmission such as channel equalization. If all modulation and demodulation filters are of length $L = gK$, and only the delay involved in the convolutions are considered, then $d = g$. In the following, the constellation points of $\mathbf{Y}_{p_1}(n_1 + d)$ is derived.

Theorem 1: Given a J -dimensional vector symbol transmitted in time frame n_1 , $\mathbf{X}_{p_1}(n_1)$, as defined in Eq. (5.3), the constellation points $\mathbf{S}_{p_1} = [s_{p_1}, s_{p_1+1}, \dots, s_{p_1+J-1}]^T$, of the corresponding received vector symbol $\mathbf{Y}_{p_1}(n_1 + d)$, as defined in Eq. (5.4), can be determined as:

$$\mathbf{S}_{p_1} = \mathbf{A} \cdot \mathbf{X}_{p_1}(n_1), \quad (5.5)$$

where

$$\mathbf{A} = \begin{bmatrix} \alpha_{p_1 p_1}(n_1) & \alpha_{p_1(p_1+1)}(n_1) & \cdots & \alpha_{p_1(p_1+J-1)}(n_1) \\ \alpha_{p_2 p_1}(n_1) & \alpha_{p_2(p_1+1)}(n_1) & \cdots & \alpha_{p_2(p_1+J-1)}(n_1) \\ \vdots & \vdots & \ddots & \vdots \\ \alpha_{(p_1+J-1)p_1}(n_1) & \alpha_{(p_1+J-1)(p_1+1)}(n_1) & \cdots & \alpha_{(p_1+J-1)(p_1+J-1)}(n_1) \end{bmatrix}, \quad (5.6)$$

$\alpha_{p_m p_n}$, $p_m \in \mathcal{P}(p_1)$ and $p_n \in \mathcal{P}(p_1)$, is calculated as follows

$$\alpha_{p_m p_n}(n_1) = \sum_{j=0}^{L_c-1} c(j) \sum_{l=0}^{L-1} f_{p_m}(l) h_{p_n}(-j-l), \quad (5.7)$$

where L_c is the length of the communication channel $c(n)$.

Proof: Without loss of generality, the subchannel p_1 is taken as a sample subchannel for the following analysis. According to the **Formulation 1** in Section 4.1.2, the received symbol of subchannel p_1 at time frame n_1 , $y_{p_1}(n_1 + d)$, can be expressed as:

$$y_{p_1}(n_1 + d) = \xi + \alpha_{p_1 p_1}(n_1)x_{p_1}(n_1) + \sum_{p \neq p_1, p=0}^{P-1} \sum_n \alpha_{pp_1}(n)x_p(n) + \sum_{n, n \neq n_1} \alpha_{p_1 p_1}(n)x_{p_1}(n). \quad (5.8)$$

where $\alpha_{pp_1}(n)$ is defined in Eq. (4.12). The first term on the righthand side of Eq. (5.8), ξ is the contribution from the additive channel noise and it can be calculated as

$$\xi = \sum_{n=-\infty}^{\infty} e(n)h_{p_1}(n_1 K - n). \quad (5.9)$$

By rearranging the last three items on the right handside of Eq. (5.8), we get an alternative expression for $y_{p_1}(n_1 + d)$

$$y_{p_1}(n_1 + d) = \sum_{p, p \in \mathcal{P}(p_1)} \alpha_{pp_1}(n_1)x_p(n_1) + \sum_{n, n \neq n_1} \sum_p \alpha_{pp_1}(n)x_p(n) + \sum_{p, p \notin \mathcal{P}(p_1)} \alpha_{pp_1}(n_1)x_p(n_1) + \xi, \quad (5.10)$$

Note that all the J transmitted symbols in subset p_1 , $\{x_{p_1}(n), x_{p_1+1}(n), \dots, x_{p_1+J-1}(n)\}$, are deterministic, hence the first term on the righthand side of Eq. (5.10) is deterministic given that the modulation/demodulation filters and transmission channel are linear and time invariant. The second and third terms in Eq. (5.10) are random processes which are interference involved in the received symbol $y_{p_1}(n_1 + d)$. Denote the interference item as ς_{p_1} , which can be calculated as

$$\varsigma_{p_1} = \sum_{n, n \neq n_1} \sum_p \alpha_{pp_1}(n)x_p(n) + \sum_{p, p \notin \mathcal{P}(p_1)} \alpha_{pp_1}(n_1)x_p(n_1), \quad (5.11)$$

i.e., ς_{p_1} is the weighted sum of identical independent distributed (iid) random variables, $x_p(n)$, $0 \leq p \leq P - 1$. According to the Central Limit Theorem [35], ς_{p_1} approaches a Gaussian random process as the quantity of $x_p(n)$, which is mainly dominated by P , gets large. Moreover, the mean and variance of ς_{p_1} can be calculated as:

$$\mu_{\varsigma_{p_1}} = \sum_{n, n \neq n_1} \sum_p \alpha_{pp_1}(n)E[x_p(n)] + \sum_{p, p \notin \mathcal{P}(p_1)} \alpha_{pp_1}(n_1)E[x_p(n_1)], \quad (5.12)$$

$$\sigma_{\varsigma_{p_1}}^2 = \sum_{n, n \neq n_1} \sum_p |\alpha_{pp_1}(n)|^2 \text{Var}[x_p(n)] + \sum_{p, p \notin \mathcal{P}(p_1)} |\alpha_{pp_1}(n_1)|^2 \text{Var}[x_{p_1}(n_1)], \quad (5.13)$$

where $E[\cdot]$, $\text{Var}[\cdot]$ and $|\cdot|$ respectively denote the expected value, the variance and the absolute value. Assume all transmitted symbols, $x_p(n)$, $0 \leq p \leq P-1$, are modulated with MPSK scheme, where $x_p(n)$ is coded as

$$x_p(n) = \sqrt{\epsilon_x} e^{j\theta_k}, \quad k = 0, 1, \dots, M-1, \quad (5.14)$$

where θ_k is the transmitted phase and will take on one of the values from the set $\{(2\pi k)/M\}$. Without loss of generality, assume

$$E[x_p(n)] = 0, \quad (5.15)$$

and from Eq. (5.14) that

$$\text{Var}[x_p(n)] = \epsilon_x, \quad (5.16)$$

for $p = 0, 1, \dots, P-1$. The mean and variance of Gaussian random variable ς_{p_1} can be obtained as:

$$\mu_{\varsigma_{p_1}} = 0, \quad (5.17)$$

$$\sigma_{\varsigma_{p_1}}^2 = \left[\sum_{n, n \neq n_1} \sum_p |\alpha_{pp_1}(n)|^2 + \sum_{p, p \notin \mathcal{P}(p_1)} |\alpha_{pp_1}(n_1)|^2 \right] \epsilon_x, \quad (5.18)$$

It is easy to see from Eq. (5.9) that ξ is a Gaussian random process with zero mean and variance

$$\sigma_{\xi}^2 = \sigma_n^2, \quad (5.19)$$

where σ_n^2 is the variance of additive channel noise.

Consequently, the mean of $y_{p_1}(n_1)$, which is also the constellation point of the received symbol on subchannel p_1 , $s_{p_1}(n_1)$, can be calculated as

$$\begin{aligned} s_{p_1} = E[y_{p_1}(n_1)] &= \sum_{p, p \in \mathcal{P}(p_1)} \alpha_{pp_1}(n_1) x_p(n_1) \\ &= \left[\alpha_{p_1 p_1}(n_1) \quad \cdots \quad \alpha_{p_1(p_1+J-1)}(n_1) \right] \mathbf{X}_{p_1}(n_1). \end{aligned} \quad (5.20)$$

The variance of $y_{p_1}(n_1 + d)$ can be calculated as

$$\sigma_{y_{p_1}}^2 = \sigma_{\xi}^2 + \sigma_{\varsigma_{p_1}}^2. \quad (5.21)$$

Using Eqs. (5.18) and (5.19), we get

$$\sigma_{y_{p_1}}^2 = \left[\sum_{n, n \neq n_1} \sum_p |\alpha_{pp_1}(n)|^2 + \sum_{p, p \notin \mathcal{P}(p_1)} |\alpha_{pp_1}(n_1)|^2 \right] \epsilon_x + \sigma_n^2. \quad (5.22)$$

The constellation point for the subchannel p_m , $p_m \in \mathcal{P}(p_1)$, can be obtained by substituting p_m for p_1 in Eq. (5.20) as

$$\begin{aligned} s_{p_m} = E[y_{p_m}(n_1)] &= \sum_{p, p \in \mathcal{P}(p_1)} \alpha_{pp_m}(n_1) x_p(n_1) \\ &= \left[\alpha_{p_m p_1}(n_1) \quad \alpha_{p_m(p_1+1)}(n_1) \quad \cdots \quad \alpha_{p_m(p_1+J-1)}(n_1) \right] \cdot \mathbf{X}_{p_1}(n_1) \end{aligned} \quad (5.23)$$

Eq. (5.5) can be obtained by putting Eq. (5.20) and Eq. (5.23) in matrix format. **Theorem 1** is proved.

Remark: When filter bank modulator/demodulator and the transmission channel are both known, \mathbf{S}_{p_1} is deterministic. Each element of \mathbf{S}_{p_1} is a weighted sum of transmitted symbols in subset p_1 and all weights are constant. Therefore in general, corresponding to each constellation point of the transmitted vector symbol $\mathbf{X}_{p_1}(n_1)$, there exists one and only one constellation point for the received vector symbol \mathbf{S}_{p_1} . The constellation points of $\mathbf{X}_{p_1}(n_1)$ and \mathbf{S}_{p_1} are a one-to-one mapping. All the values that \mathbf{S}_{p_1} can take form the constellation set of the received J -dimensional vector symbol $\mathbf{Y}_{p_1}(n_1 + d)$, which is denoted as C_s . The cardinality of the alphabet set of \mathbf{S}_{p_1} is same as that of the alphabet set of $\mathbf{X}_{p_1}(n_1)$, G .

A received OFDM symbol consists of the received symbols from all P subchannel. The derivation of the constellation points of a received OFDM symbol is a special case of **Theorem 1**. Assigning the constellation points of the received OFDM symbol, $\{y_0(n_1 + d), y_1(n_1 + d), \dots, y_{P-1}(n_1 + d)\}$, as $\mathbf{S} = [s_0, s_1, \dots, s_{P-1}]^T$, which can be calculated as

$$\mathbf{S} = \begin{bmatrix} \alpha_{00}(n_1) & \alpha_{01}(n_1) & \cdots & \alpha_{0(P-1)}(n_1) \\ \alpha_{10}(n_1) & \alpha_{11}(n_1) & \cdots & \alpha_{1(P-1)}(n_1) \\ \vdots & \vdots & \ddots & \vdots \\ \alpha_{(P-1)0}(n_1) & \alpha_{(P-1)1}(n_1) & \cdots & \alpha_{(P-1)(P-1)}(n_1) \end{bmatrix} \cdot \begin{bmatrix} x_0(n_1) \\ x_1(n_1) \\ \vdots \\ x_{P-1}(n_1) \end{bmatrix}. \quad (5.24)$$

5.1.3 Joint Detection of Received Vector Symbol

For a given subset p_1 , the task of the subset joint detection can be described as to find the constellation point in C_S for $\mathbf{Y}_{p_1}(n_1 + d)$ based on ML criterion, then decide which constellation point in C_X is transmitted on basis of the one-to-one mapping relation of C_S and C_X . According to ML criterion, the $\mathbf{Y}_{p_1}(n_1 + d)$ should be decoded as $\mathbf{S}_{p_1}^i, i = 1, 2, \dots, G$, which maximizes the conditional PDF $f_{\mathbf{Y}|\mathbf{S}}(\mathbf{Y}_{p_1}|\mathbf{S}_{p_1}^i)$. In the following this conditional PDF function is derived.

Theorem 2: Given the transmitted vector symbol $\mathbf{X}_{p_1}(n_1)$, as defined in Eq. (5.3), and the constellation point of the corresponding received vector symbol $\mathbf{Y}_{p_1}(n_1 + d)$, $\mathbf{S}_{p_1}^i$, the conditional PDF function $f_{\mathbf{Y}|\mathbf{S}}(\mathbf{Y}_{p_1}|\mathbf{S}_{p_1}^i)$ can be expressed as

$$f_{\mathbf{Y}|\mathbf{S}}(\mathbf{Y}_{p_1}|\mathbf{S}_{p_1}^i) = \frac{1}{(2\pi)^{J/2}|\Sigma|^{1/2}} \exp \left[-\frac{1}{2}(\mathbf{Y}_{p_1} - \mathbf{S}_{p_1}^i)^H \Sigma^{-1}(\mathbf{Y}_{p_1} - \mathbf{S}_{p_1}^i) \right], \quad (5.25)$$

where Σ is a diagonal matrix which is defined as

$$\Sigma = \begin{bmatrix} \sigma_{y_{p_1}}^2 & 0 & \cdots & 0 \\ 0 & \sigma_{y_{p_1+1}}^2 & \cdots & 0 \\ \vdots & \vdots & \ddots & \vdots \\ 0 & 0 & \cdots & \sigma_{y_{(p_1+J-1)}}^2 \end{bmatrix}, \quad (5.26)$$

where $\sigma_{y_{p_m}}^2$, the sum of variance of channel noise and interference in subchannel p_m , $p_m \in \mathcal{P}(p_1)$, can be calculated by substituting p_m for p_1 in Eq. (5.22).

Proof: The statistical characteristics of the element $p_m, p_m \in \mathcal{P}(p_1)$ of $\mathbf{Y}_{p_1}(n_1 + d)$, $y_{p_m}(n_1 + d)$, is considered. As explained in Theorem 1, $y_{p_m}(n_1 + d)$ is a Gaussian random variable with mean s_{p_m} and variance

$$\sigma_{y_{p_m}}^2 = \sigma_{\xi}^2 + \sigma_{\zeta_{p_m}}^2. \quad (5.27)$$

Therefore, the conditional PDF of $y_{p_m}(n_1 + d)$, given the transmitted symbol which corresponding to constellation point $s_{p_m}^i$, can be obtained as:

$$f_y(y_{p_m}|s_{p_m}^i) = \frac{1}{\sqrt{2\pi}\sigma_{y_{p_m}}^2} \exp \left[-\frac{(y - s_{p_m}^i)^2}{2\sigma_{y_{p_m}}^2} \right], \quad (5.28)$$

In the following we will demonstrate that $y_{p_m}(n_1 + d)$, $p_m \in \mathcal{P}(p_1)$ is independent to symbols received on the other subchannels of subset p_m during the same frame, $y_{p_j}(n_1 + d)$, $p_j \in \mathcal{P}(p_1)$ and $p_j \neq p_m$. According to Eq. (4.15), $y_{p_j}(n_1 + d)$ can be expressed as

$$y_{p_j}(n_1 + d) = \sum_l r(l)h_{p_j}(n_1K - l), \quad (5.29)$$

and

$$y_{p_m}(n_1 + d) = \sum_k r(k)h_{p_m}(n_1K - k), \quad (5.30)$$

the correlation function of $y_{p_m}(n_1 + d)$ and $y_{p_j}(n_1 + d)$, $R_{yy}(l, k)$ is

$$\begin{aligned} R_{yy}(l, k) &= E[y_{p_m}(n_1 + d)y_{p_j}^*(n_1 + d)] \\ &= \sum_l \sum_k E[r(l)r^*(k)]h_{p_m}(n_1K - l)h_{p_j}^*(n_1K - k). \end{aligned} \quad (5.31)$$

From Eqs. (5.1) and (5.2) that, in an OFDM system, the modulation filters and their K -shifted versions form a set of orthonormal basis, so do the demodulation filters. When the frequency bandwidth of the subset p_1 is sufficiently narrow compared to the bandwidth of the transmission channel, it is reasonable to assume that $E[r(l)r^*(k)] = \delta(l - k)$ within the bandwidth of the subset, then

$$R_{yy}(l, k) = 0, \quad \text{for } p_m \neq p_j, \quad (5.32)$$

i.e. $y_{p_m}(n_1 + d)$ and $y_{p_j}(n_1 + d)$ are uncorrelated. From Eq. (5.32), $\mathbf{Y}_{p_1}(n_1 + d)$ is a J -dimensional joint-Gaussian random variable vector consisting of J independent one-dimensional Gaussian random variables $y_{p_1}(n_1), y_{p_1+1}(n_1), \dots, y_{p_1+J-1}(n_1)$. The conditional joint PDF of \mathbf{Y}_{p_1} , given the transmitted vector symbol which corresponds to constellation point $\mathbf{S}_{p_1}^i$, can be obtained

$$f_{\mathbf{Y}|\mathbf{S}}(\mathbf{Y}_{p_1}|\mathbf{S}_{p_1}^i) = \prod_{p_m, p_m \in \mathcal{P}}^{p_1+J-1} f_{y|s}(y_{p_m}|s_{p_m}^i). \quad (5.33)$$

By substituting Eq. (5.28) for (5.33), **Theorem 2** is proved.

The Mahalanobis distance from the distorted vector symbol $\mathbf{Y}_{p_1}(n_1 + d)$ to the constellation point $\mathbf{S}_{p_1}^i$ is defined as [43]

$$MD(\mathbf{Y}_{p_1}, \mathbf{S}_{p_1}^i) = (\mathbf{Y}_{p_1} - \mathbf{S}_{p_1}^i)^H \Sigma^{-1} (\mathbf{Y}_{p_1} - \mathbf{S}_{p_1}^i) \quad (5.34)$$

By applying ML detection algorithm, we decode $\mathbf{Y}_{p_1}(n_1 + d)$ as the constellation point $\mathbf{S}_{p_1}^i$ which maximizes conditional PDF $f_{\mathbf{Y}|\mathbf{S}}(\mathbf{Y}_{p_1}|\mathbf{S}_{p_1}^i)$. This is equivalent to decode $\mathbf{Y}_{p_1}(n_1 + 1)$ by the Mahalanobis distance, defined in Eq. (5.34), between $\mathbf{Y}_{p_1}(n_1 + d)$ and each constellation point $\mathbf{S}_{p_1}^i, i = 0, 1, \dots, G - 1$, and assign $\mathbf{Y}_{p_1}(n_1 + d)$ to be the constellation point for which the Mahalanobis distance is the minimum. Then according to the one-to-one mapping between the constellation point set of the received vector symbol, C_S , and the constellation point set of the transmitted vector symbol, C_X , the transmitted vector symbol are figured out. The detection process is schematically shown in Fig. 5.2.

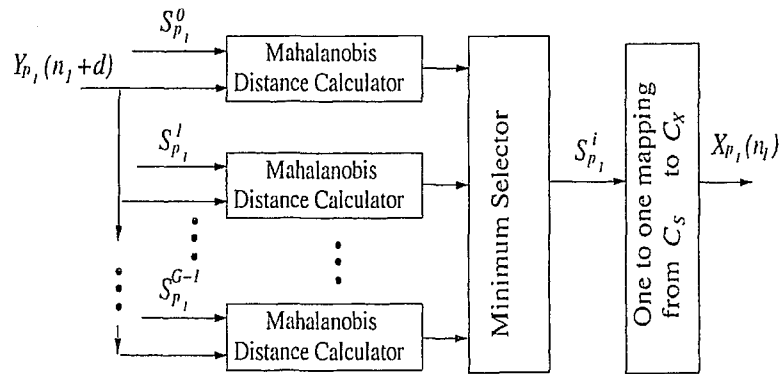


Figure 5.2: Schematic illustration of ML detector

5.1.4 Error Performance Analysis

The formulation of the average error probability of received J -dimensional vector symbol $\mathbf{Y}_{p_1}(n_1 + g)$, denoted as VSER P_{ve,p_1} , is theoretically straightforward. An error occurs whenever the received vector symbol $\mathbf{Y}_{p_1}(n_1 + g)$ does not fall inside region $R_{p_1}^i$, which is associated with the constellation point $\mathbf{S}_{p_1}^i$ [44], and the VSER can be calculated as

$$P_{ve,p_1} = 1 - \frac{1}{G} \sum_{l=0}^{G-1} \int_{R_{p_1}^l} f_{\mathbf{Y}|\mathbf{S}}(\mathbf{Y}_{p_1}|\mathbf{S}_{p_1}^l) d\mathbf{Y}_{p_1}, \quad (5.35)$$

However, the decision on the boundary of $R_{p_1}^i$ and the numerical computation of Eq. (5.35) are not feasible in most cases. In the following, an upper bound is derived for the VSER by

transforming the Mahalanobis distances between $\mathbf{Y}_{p_1}(n_1 + g)$ and $\mathbf{S}_{p_1}^i$, $i = 0, 1, \dots, G-1$, to the Euclidean distances between a new observation vector and new vector constellation points.

The inverse of the $J \times J$ diagonal matrix Σ can be decomposed as

$$\Sigma^{-1} = \mathbf{B}^H \mathbf{B}, \quad (5.36)$$

where \mathbf{B} is also a $J \times J$ diagonal matrix which is defined as

$$\mathbf{B} = \text{diag} \left\{ \frac{1}{\sigma_{y_{p_1}}}, \frac{1}{\sigma_{y_{p_1+1}}}, \dots, \frac{1}{\sigma_{y_{(p_1+J-1)}}} \right\}. \quad (5.37)$$

By substituting Eq. (5.37) into Eq. (5.34), the following expression is obtained that

$$MD(\mathbf{Y}_{p_1}, \mathbf{S}_{p_1}^i) = -(\mathbf{B}\mathbf{Y}_{p_1} - \mathbf{B}\mathbf{S}_{p_1}^i)^H (\mathbf{B}\mathbf{Y}_{p_1} - \mathbf{B}\mathbf{S}_{p_1}^i). \quad (5.38)$$

Assign the new observation vector symbol as

$$\mathbf{Z}_{p_1} = \mathbf{B}\mathbf{Y}_{p_1}, \quad (5.39)$$

and the new constellation point as

$$\mathbf{V}_{p_1}^i = \mathbf{B}\mathbf{S}_{p_1}^i, \quad (5.40)$$

in spatial domain, the Gaussian random noise in each one of J orthogonal directions is changed into AWGN noise with unit power. The AWGN noise processes in the J directions are iid noise processes. It is easy to see that

$$MD(\mathbf{Y}_{p_1}, \mathbf{S}_{p_1}^i) = UD(\mathbf{Z}_{p_1}, \mathbf{V}_{p_1}^i). \quad (5.41)$$

where $UD(\mathbf{Z}_{p_1}, \mathbf{V}_{p_1}^i)$ is the Euclidean distance between \mathbf{Z}_{p_1} and $\mathbf{V}_{p_1}^i$. By replacing the Mahalanobis distance between \mathbf{Y}_{p_1} and $\mathbf{S}_{p_1}^i$ to the Euclidean distance between \mathbf{Z}_{p_1} and $\mathbf{V}_{p_1}^i$, the task of finding an $\mathbf{S}_{p_1}^i$ which is closest to \mathbf{Y}_{p_1} in terms of Mahalanobis distance change to finding a $\mathbf{V}_{p_1}^i$ which is closest to \mathbf{Z}_{p_1} in terms of Euclidean distance, and \mathbf{Z}_{p_1} is a J -dimensional observation vector distorted by iid AWGN noise in each of the J directions. The variance matrix of \mathbf{Z}_{p_1} is a $J \times J$ identity matrix.

On basis of [44], the upper bound of the average probability of vector symbol error, P_{ve,p_1} , only depends on the minimum Euclidean distance between any pair of the constellation points, $V_{p_1}^i$ and $V_{p_1}^k$, $1 \leq i, k \leq G$, $i \neq k$, and the power of the iid AWGN noise. In the case that the AWGN noise having unit power, the upperbound of the average probability of the VSER can be calculated as

$$P_{ve,p_1} \leq \frac{G-1}{2\sqrt{\pi}} \exp\left(-\frac{d_{min}^2}{2}\right). \quad (5.42)$$

where

$$d_{min} = \min_{k \neq i} UD(V_{p_1}^i, V_{p_1}^k), \quad for 1 \leq i, k \leq G. \quad (5.43)$$

Eq. (5.42) shows that, P_{ve,p_1} decreases exponentially as the square minimum distance of the transformed constellation points, d_{min}^2 , increases.

Thus far, VSER has been the only figure used in the proposed joint detection algorithm to assess the error performance of a generic OFDM system. However, it is also meaningful to evaluate the SER, P_e , of the one-dimensional symbol received on one of P subchannels, under joint detection algorithm. The relation of P_{ve,p_1} and P_{e,p_1} , the SER of subchannel p_i , $p_i \in \mathcal{P}(p_1)$, is explained in the following.

$$\begin{aligned} P_{ve,p_1} &= P\left(\bigcup_{p_i=p_1}^{p_1+J-1} (\text{subchannel } p_i \text{ is in error})\right) \\ &\leq \sum_{p_i=p_1}^{p_1+J-1} P_{e,p_i}, \end{aligned} \quad (5.44)$$

where \cup represents the union operation. We also note that

$$P_{ve,p_1} \geq P(\text{subchannel } p_i \text{ is in error}) = P_{e,p_i}. \quad (5.45)$$

It follows therefore that the SER in the subset p_1 is bounded as follows:

$$\frac{P_{ve,p_1}}{J} \leq P_{e,p_i} \leq P_{ve,p_1}. \quad (5.46)$$

The SER over all P subchannels, P_e , can be evaluated by averaging P_{ve,p_i} over all the P/J subsets:

$$\frac{\sum_{p_1=1}^{P/J} P_{ve,p_1}}{P} \leq P_e \leq \sum_{p_1=1}^{P/J} P_{ve,p_1}. \quad (5.47)$$

5.1.5 Discussions

For AWGN channels or channels which have been perfectly equalized, the transfer function $c(n) = \delta(n)$, there is no ISI and ICI involved in the received symbols due to the PR property of the filter bank modulator and demodulator. The only distortion in received symbols comes from additive channel noise. Therefore the Σ in Eq. (5.25) is reduced to

$$\Sigma = \begin{bmatrix} \sigma_n^2 & 0 & \cdots & 0 \\ 0 & \sigma_n^2 & \cdots & 0 \\ \vdots & \vdots & \ddots & \vdots \\ 0 & 0 & \cdots & \sigma_n^2 \end{bmatrix}, \quad (5.48)$$

where σ_n^2 is the variance of the channel noise. For AWGN channels, from Eq. (5.48) that the noises in all J orthogonal directions are iid. noise with variance σ_n^2 , and the Euclidean distance can be employed directly for ML detection. Moreover, for AWGN channels, it is possible to do further exploration on the constellation points of the received vector symbol $\mathbf{Y}_{p_1}(n_1 + d)$. The matrix \mathbf{A} in Eq. (5.5) can be verified as an identity matrix by substituting Eq. (5.2) into (5.6). Consequently the constellation points of the received vector symbol $\mathbf{Y}_{p_1}(n_1 + d)$ are same as that of transmitted symbols $\mathbf{X}_{p_1}(n_1)$. For AWGN channels, an OFDM system demonstrates same error performance under joint detection algorithm and subchannel detection algorithm.

5.2 Simulations

System simulations are implemented to evaluate the performance of various OFDM systems by employing the proposed joint detection algorithm. In the simulations, all subchannel symbols are modulated with the BPSK scheme. The P subchannels are divided into a number of disjoint subsets, with each subset including 8 subchannels, for BPSK modulation.

In system simulations, the composite transmitted signal to be transmitted through the channel, $s(n)$, as illustrated in Fig. 5.1, is obtained by first upsampling each of the p BPSK symbols streams $\{x_0(n), x_1(n), \cdots, x_{P-1}(n)\}$ by factor K , then convolving with one of the

P modulation filters, finally summing up all output from P subchannels. After the $s(n)$ convolving with the transmission channel $c(n)$, the AWGN noise is added to the composite serial symbol sequence to get the distorted signal $r(n)$. The signal $r(n)$ is then passed through the demodulation filter of each subchannel, and the result signal on each subchannel is downsampled by factor K . The P received symbols, $\{y_0(n), y_1(n), \dots, y_{P-1}(n)\}$, are divided into a number of subsets, each of size 8 for BPSK coding. The subchannel symbols in one subset, referred as a received vector symbol, are decoded jointly by calculating the Mahalanobis distances between it and all constellation points in C_S . The constellation point in C_X , which corresponding to the constellation point in C_S having the minimum Mahalanobis distances to the received vector symbol, is the one having been transmitted. To make comparison of the system error performance between the subchannel detection algorithm and the joint detection algorithm, the SER in joint detection algorithm is calculated according to the procedures outlined in Fig. 5.3. The emphasis in transferring the VSER result to SER is that, when a received vector symbol of a specific subset is not decoded correctly, each subchannel symbol in the subset will be checked with the transmitted symbol of that subchannel to see whether this received subchannel symbol is correctly decoded. By considering all received vector symbols that are wrongly decoded in the way described above, we obtain the simulated average SER.

Numerical simulations are performed with three kinds of OFDM systems, namely, the DFT-based OFDM system with zero-padded CP, the DFT-based OFDM without CP and the conventional DWMT system overlapping factor $g = 2$ whose modulation filter are generated from the prototype filter defined in Eq. (4.56). The sample channels include an AWGN channel and two fading channels with impulse response $c_1(n) = [1, 0.5e^{j\pi/6}]$ and $c_2(n) = [1, 0.5e^{j\pi/6}, 0.3e^{-j\pi/3}, 0.2e^{j\pi/2}, 0.1]$.

Fig. 5.4 show numerical simulation results of both subchannel detection and joint detection for OFDM systems over AWGN channels. Both detection algorithms have same error performance which is not changed with the number of subchannels, P .

Fig. 5.5 and Fig. 5.6 demonstrate error performance of both detection algorithms under

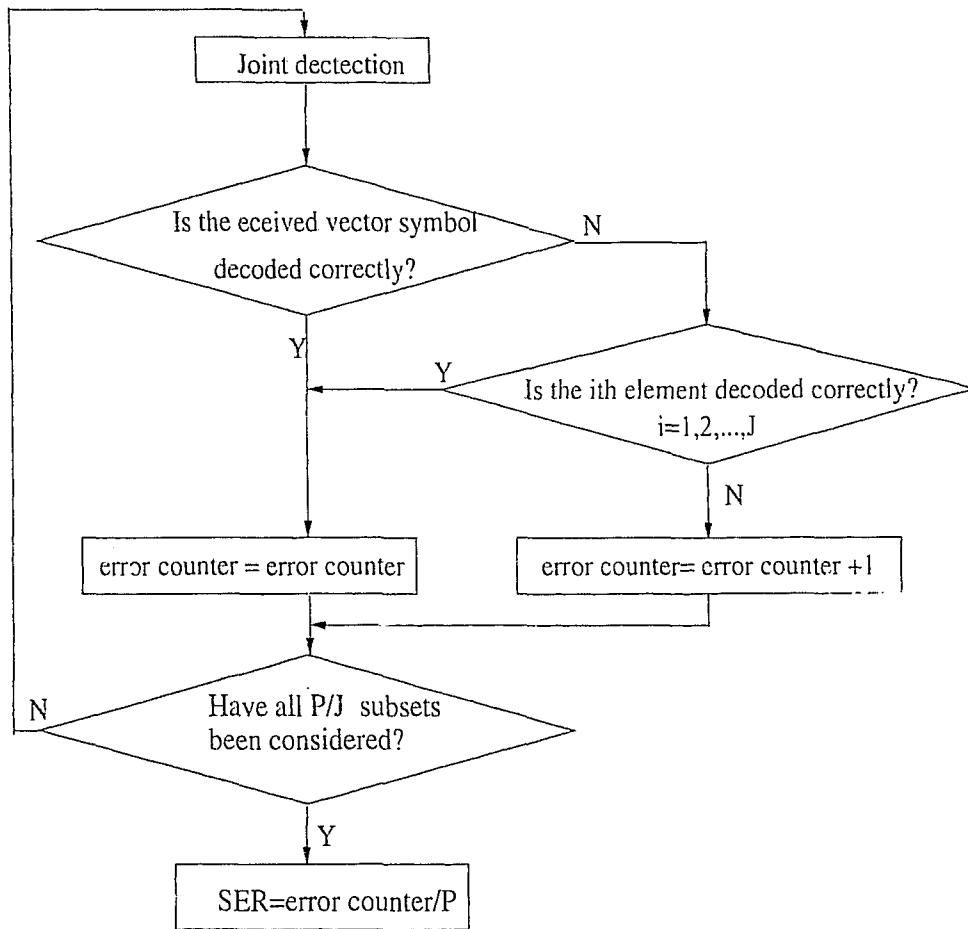


Figure 5.3: Calculation of SER under joint detection algorithm

the two sample fading channels. These figures demonstrate that joint detection algorithm has superior performance than subchannel detection algorithm especially when the SNR getting larger.

5.3 Summary

In this chapter, a joint maximum likelihood detection algorithm is proposed to jointly detect and decode the symbols received during one time frame. By employing the joint detection algorithm, the effects of symbols in the same time frame are used to calculate the constellation points of the received vector symbols instead of being considered

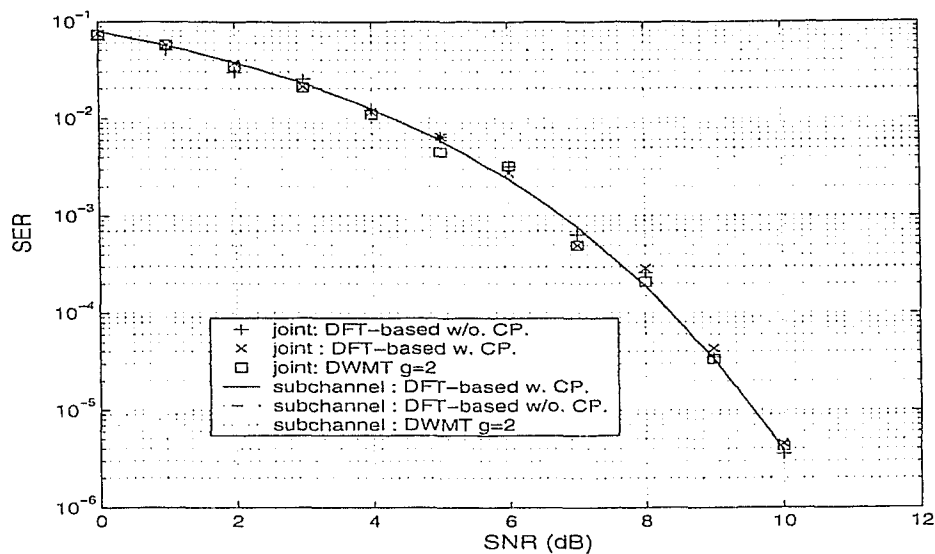


Figure 5.4: Comparison of joint detection and subchannel detection over an AWGN channel with BPSK ($P = 32$)

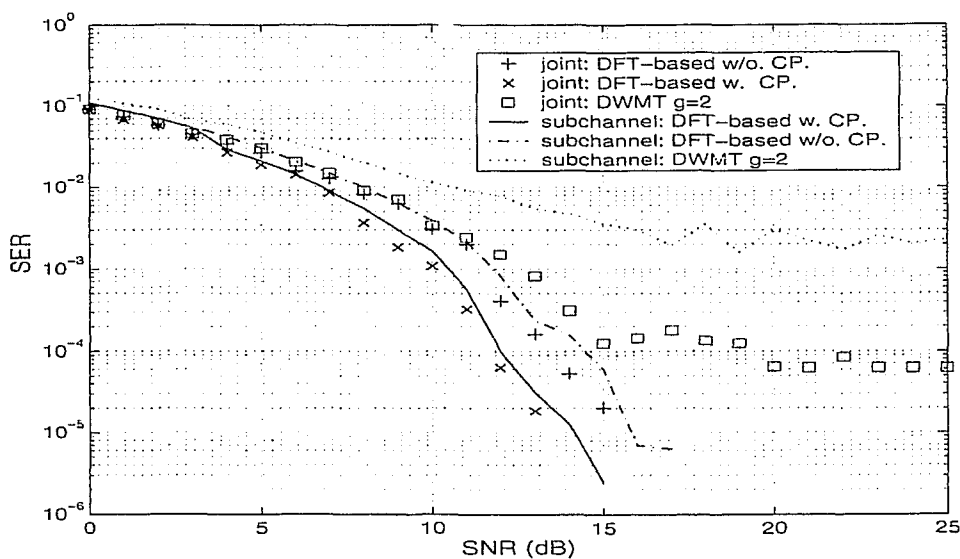


Figure 5.5: Comparison of joint detection and subchannel detection over channel $c_1(n)$ with BPSK ($P = 32$)

as interference in subchannel detection algorithm. An upper bound of VSER is derived by transferring Mahalanobis distances, between the received vector symbol and the con-

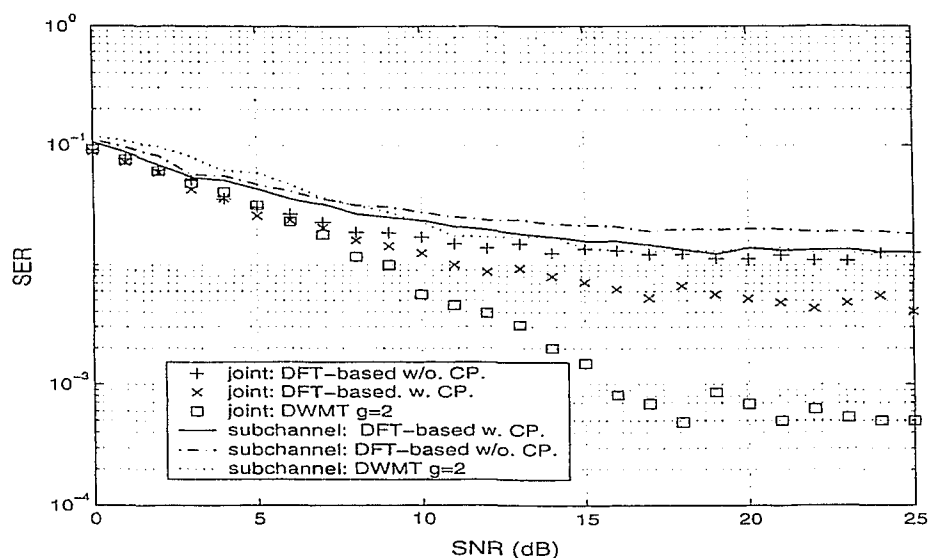


Figure 5.6: Comparison of joint detection and subchannel detection over channel $c_2(n)$ with BPSK ($P = 32$)

stellation points of the received vector symbol, to the the Euclidean distances of a new observation vector and new constellation points, to provide a practical viewpoint of the system performance under joint detection algorithm. Monte-Carlo numerical simulations are performed, with the DFT-based OFDM systems and DWMT systems, to compare the performances of the subchannel and the joint detection algorithms. Simulation results demonstrate that the proposed joint detection algorithm has better error performance for an OFDM system than the subchannel detection algorithm.

Chapter 6

Conclusions and Future Research

6.1 Conclusions

In a generic OFDM system, modulation filters form a set of orthonormal basis, and modulation filters and demodulation filters fulfill the perfect reconstruction property to keep subchannels well isolated, and enable the transmitted symbols to be perfectly retrieved from the received symbols. However, in most cases these nice properties are easily destroyed by multipath channels. Some work has been done in evaluating the error performance for the DFT-based OFDM systems. The topics unaddressed in the published literature include the systematical error performance evaluation for a *generic* OFDM system, and some detection algorithms other than the subchannel detection algorithm, in which each received symbol is detected individually without considering all information carried by the other symbols. Both of the subjects are addressed in this study.

Firstly in this study, a closed-form formula of the SER has been derived for MPSK coded OFDM systems which employs optimum phase detection for each subchannel. The derivation of the SER formula is based on the constellation points of the received symbols and the assumption that the sum of ISI and ICI can be modelled as a Gaussian random process when the number of subchannels is large. This formula can be used to calculate the SER of either the DFT-based OFDM system, the DWMT system or other OFDM systems which fulfill the orthogonality and PR requirements and use MPSK modulation. The applications of the derived formula in AWGN channels and fading channels are discussed.

Results of numerical simulations demonstrate the consistency with the SER formula over both AWGN and fading channels.

Secondly, a systematic method is presented to design a novel OFDM system based on complex-valued multiband unitary filter banks, which have more flexible frequency response and are more suitable to deal with complex-valued signals present in wireless systems. This method provides flexibilities in choosing OFDM subchannels for different applications by optimizing filter banks towards different objective functions. In this thesis, the derived SER formula, for a generic MPSK-OFDM system, is employed as the objective function. System simulations show that the designed OFDM system outperforms DWMT systems, filters of both systems are of the same length, in terms of SER. Simulations also show that the error performance of the designed OFDM system is comparable to DFT-based OFDM with zero-padded cyclic prefix, which compromise the transmission rate for better error performance.

Finally in this study, a joint ML detection algorithm is proposed to jointly detect and decode the symbols received at one time frame. The received symbols in one frame are partitioned into several subsets, and the received symbols within one subset are decoded jointly. The joint detection algorithm make better use of the information carried by the other symbols in the same subset as the one to be decoded, and comparatively reduces the interference involved in the symbol to be detected. Based on the constellation points and the PDF function of the received vector symbol, an upper bound of the VSER is derived by transferring the Mahalanobis distances between the received vector symbol and the constellation points of the received vector symbol to the Euclidean distances of a new transferred observation vectors and the new transferred constellation points. Monte-Carlo numerical simulation are performed, with the DFT-based OFDM and DWMT systems, to compare the performances of the subchannel detection algorithm and the joint detection algorithm. Simulation results demonstrates that the joint detection algorithm provides better error performance for an OFDM system than the subchannel detection algorithm.

6.2 Future Research

OFDM has a promising future in wireless local area network and in fixed and mobile communications due to its high spectral efficiency and flexibility in spectrum allocation and modulation.

Further work could be done under both the subchannel and the joint detection algorithms for the detection and error performance evaluation for a generic OFDM system.

Under the subchannel detection algorithm, the overall effect of channel noise and interference for a given subchannel is approximated as a zero-mean Gaussian process in the **Formulation 1** of chapter 4. The constellation points of received symbol and its PDF function can both be derived from the constellation points of the transmitted symbol. In this way, the error performance evaluation is mainly based on the detectors and the decoding decision boundaries at the receiver end of each subchannel. In Chapter 4, the SER formula for the MPSK modulation is derived. The other modulation schemes in a OFDM system include QAM and M-ary differential phase shift keying (MDPSK), to name two. The formulation for SER expressions for these modulation schemes will be done in the future.

Under the proposed joint detection algorithm, the ICI is partially eliminated by jointly decoding the received symbols within a subset (Chapter 5). However, the joint detection algorithm can be extended to jointly detect successive symbols for a given subchannel, hence partially reducing the ISI, or jointly detect all symbols in a subset within a number of successive frame to partially reduce both ICI and ISI.

In the simulation studies, the fading channels are randomly selected and are comparatively simple. In the future, the Rayleigh and Rice fading channels will be adopted to evaluate system performance in practical situations.

Appendix A

Central Limit Theorem

This appendix is a summary of the central limit theorem on basis of [45].

The common definition of the central limit theorem consider the normalized sum of a large number of identically distributed random variables x_i , where y is the normalized random variable given by

$$y = \frac{1}{\sqrt{M}} \sum_{i=0}^{M-1} (x_i - \mu) \quad (\text{A.1})$$

and each x_i has mean μ and variance σ^2 . The random variable y is approximately normally distributed (a Gaussian distribution with zero mean and unit variance) as M becomes large.

A more general statement of the central limit theorem justify the Gaussian approximation when x_i , $i = 0, 1, \dots, M - 1$, are not identically distributed but are independent. It requires that the sum

$$y = \sum_{i=0}^{M-1} x_i \quad (\text{A.2})$$

of M random variables, x_i (which are not necessarily identically distributed but are independent), each with mean μ_{x_i} and variance $\sigma_{x_i}^2$, approaches a Gaussian random variable as M gets large, provided that

$$\sigma_{x_j}^2 \ll \sigma_y^2 = \sum_{i=0}^{M-1} \sigma_{x_i}^2, \quad (\text{A.3})$$

for $j = 0, 1, \dots, M - 1$. Furthermore, the mean and variance of the sum, y , are given by

$$\mu_y = \sum_{i=1}^{M-1} \mu_{x_i}, \quad (\text{A.4})$$

$$\sigma_y^2 = \sum_{i=1}^{M-1} \sigma_{x_i}^2. \quad (\text{A.5})$$

The condition for Eq. (A.3) to hold is equivalent to specifying that no single x_i dominates y .

Appendix B

Change of Variables

The purpose of the change of variables (V, Θ_y) in Eq. (4.34) to (r, ψ_y) are to calculate SER with the integration over a finite range by applying results of [36, 37, 38, 39].

As shown in Fig. B.1, y is the received symbol, Θ_y and V are phase and radius of y , respectively. The constellation point corresponding to the transmitted symbol, with phase zero, is \bar{y}_{p_1} , y is at a distance r from \bar{y}_{p_1} and ψ_y is the angle between vectors $\overrightarrow{\bar{y}_{p_1}y}$ and $\overrightarrow{o\bar{y}_{p_1}}$ line connecting points y and \bar{y}_{p_1} and the coordinate.

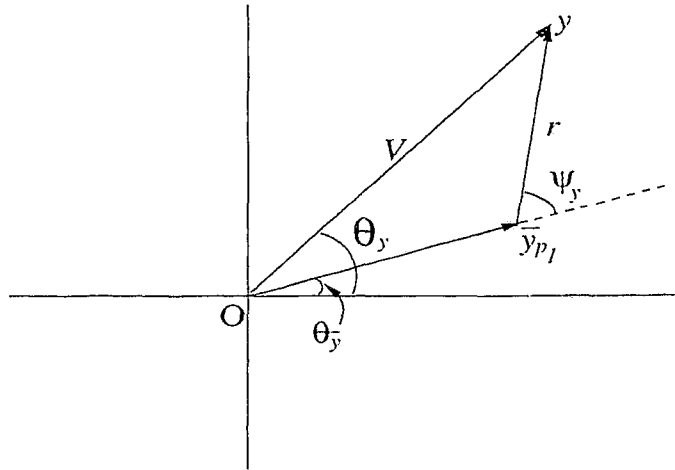


Figure B.1: Illustration of change of variables

The following expressions can be derived from Fig. B.1,

$$|\bar{y}_{p_1}| + V \cos(\Theta_y - \theta_{\bar{y}_{p_1}}) = r \cos(\psi_y), \quad (\text{B.1})$$

$$r \sin(\psi_y) = V \sin(\Theta_y - \theta_{\bar{y}_{p_1}}). \quad (\text{B.2})$$

Therefore,

$$V = \sqrt{r^2 - 2|\bar{y}_{p_1}|r \cos(\psi_y) + |\bar{y}_{p_1}|^2}, \quad (\text{B.3})$$

$$\Theta_y = \tan^{-1} \left(\frac{r \sin(\psi_y)}{r \cos(\psi_y) - |\bar{y}_{p_1}|} \right) + \theta_{\bar{y}_{p_1}}. \quad (\text{B.4})$$

or alternatively

$$r = \sqrt{V^2 + 2V \cos(\Theta_y - \theta_{\bar{y}_{p_1}})|\bar{y}_{p_1}| + |\bar{y}_{p_1}|^2}, \quad (\text{B.5})$$

$$\psi_y = \tan^{-1} \left[\frac{V \sin(\Theta_y - \theta_{\bar{y}_{p_1}})}{V \cos(\Theta_y - \theta_{\bar{y}_{p_1}}) + |\bar{y}_{p_1}|} \right]. \quad (\text{B.6})$$

According to the Change of Variable Theorem [46],

$$f_{r\psi_y}(r, \psi_y) = f_{v\Theta}(V, \Theta_y) \left| \frac{\partial(V, \Theta_y)}{\partial(r, \psi_y)} \right|, \quad (\text{B.7})$$

where $\left| \frac{\partial(V, \Theta_y)}{\partial(r, \psi_y)} \right|$ is the determinant of Jacobian matrix $\left[\frac{\partial(V, \Theta_y)}{\partial(r, \psi_y)} \right]$. Substituting Eqs. (B.3) and (B.4) into Eq. (B.7), Eq. (4.38) is obtained.

Bibliography

- [1] S. S. Pradhan and K. Ramchandran, "Efficient layered data transport over multi-carrier system using optimized embedded modulation," *IEEE Trans. on Communications*, vol. 50, pp. 877–881, June 2002.
- [2] A. N. Akansu, P. Duhamel, X. Lin, and M. Courville, "Orthogonal transmultiplexers in communications: a review," *IEEE Trans. on Signal Processing*, vol. 46, no. 4, pp. 979–995, Apr. 1998.
- [3] I. Kalet, "The multitone channel," *IEEE Trans. on Communications*, vol. 37, pp. 119–124, Feb. 1989.
- [4] V. Mignone and A. Morello, "CD3-OFDM: a novel demodulation scheme for fixed and mobile receivers," *IEEE Trans. on Communications*, vol. 44, no. 9, pp. 1144–1151, Sept. 1996.
- [5] C. Liu, "The effect of nonlinearity on a QPSK-OFDM-QAM signal," *IEEE Trans. on Consumer Electronics*, vol. 43, no. 3, pp. 443–447, Aug. 1997.
- [6] S. Lei and V. Lau, "Performance analysis of adaptive interleaving for OFDM systems," *IEEE Trans. on Vehicular Technology*, vol. 51, no. 3, pp. 435–444, May 2002.
- [7] N. Benvenuto and S. Tomasin, "On the comparison between OFDM and single carrier modulation with a DFE using a frequency-domain feedforward filter," *IEEE Trans. on Communications*, vol. 50, pp. 947–955, June 2002.

- [8] G. Cherubini, E. Eleftheriou, S. Olcer, and J. M. Cioffi, "Filter bank modulation techniques for very high-speed digital subscriber lines," *IEEE Communications Magazine*, vol. 38, no. 5, pp. 98-104, May 2000.
- [9] G. Cherubini, E. Eleftheriou, and S. Olcer, "Filtered multitone for very high-speed digital subscriber lines," *IEEE Journal on Selected Areas in Communications*, vol. 20, no. 5, pp. 1016-1028, June 2002.
- [10] P. P. Vaidyanathan, "Filter banks in digital communications," *IEEE Circuits and System Magazine*, vol. 1, no. 2, pp. 4-25, 2001.
- [11] S.B. Weinstein and P.M. Ebert, "Data transmission by frequency division multiplexing using the discrete fourier transform," *IEEE Trans. Commun. Technol.*, vol. COM-19, Oct. 1971.
- [12] M. D. Nave and C. Del-Toso, "A short overview of the VDSL system requirements," *IEEE Communications Magazine*, vol. 40, no. 12, pp. 82-90, Dec. 2002.
- [13] S. D. Sandberg and M. A. Tzannes, "Overlapped discrete multitone modulation for high speed copper wire communications," *IEEE Journal on Selected Areas in Communications*, vol. 13, no. 9, pp. 1571-1585, Dec. 1995.
- [14] M.A. Tzannes, M.C. Tzannes, and H.L. Resnikoff, "DMT systems, DWMT systems and digital filter banks," in *Proc. ICC*, vol. 1, pp. 311-315, 1994.
- [15] H. S. Malvar, "Extended lapped transforms: properties, applications, and fast algorithms," *IEEE Trans. on Signal Processing*, vol. 40, no. 11, pp. 2703-2714, Nov. 1992.
- [16] A. N. Akansu and X. Lin, "A comparative performance evaluation of DMT(OFDM) and DWMT(DSBMT) based DSL communications systems for single and multitone interference," in *proc. ICASSP*, vol. 6, pp. 3269-3272, May 1998.

- [17] W. Hwang and K. Kim. "Performance analysis of OFDM on the shadowed multipath channels," *IEEE Trans. on Consumer Electronics*, vol. 44, no. 4, pp. 1323–1328, Nov. 1998.
- [18] T. Tjhung, X. Wang, and C.S. Ng, "Error performance evaluation of the MDPSK-DMT systems in AWGN and impulse noise," *IEEE Trans. on Consumer Electronics*, vol. 46, no. 1, pp. 131–136, Feb. 2000.
- [19] T. Pollet, P. Spruyt, and M. Moeneclaey, "The BER performance of OFDM systems using non-synchronized sampling," in *Proc. IEEE GLOBECOM '94*, pp. 253–257, Nov. 1994.
- [20] G. Vandersteen, J. Verbeeck, Y. Rolain, and J. Schoukens, "Accurate bit-error-rate estimation for OFDM based telecommunication systems schemes in the presence of nonlinear distortions." in *Proc. 17th IEEE IMTC*, vol. 1, pp. 80–85, 2000.
- [21] J. Lu, T. Tjhung, F. Adachi, and C. Huang, "BER performance of OFDM-MDPSK system in frequency-selective Rician fading with diversity reception," *IEEE Trans. on Vehicular Technology*, vol. 49, no. 4, pp. 1216–1225, July 2000.
- [22] Y. Wang and X.-P. Zhang, "Symbol error rate evaluation and filter bank design for OFDM systems with MPSK modulation," *to be submitted*, 2003.
- [23] Y. Wang and X.-P. Zhang, "Design of M-band complex-valued filter banks for multicarrier transmission over multipath wireless channels," in *proc. ICASSP'03*, Apr. 2003.
- [24] Y. Wang and X.-P. Zhang, "Filter bank based interference suppression for fading channels," in *proc. CCECE'03*, May 2003.
- [25] Y. Wang and X.-P. Zhang, "Joint maximum likelihood detection algorithm for OFDM systems and error performance analysis," *to be submitted*, 2003.

- [26] P. P. Vaidyanathan, *Multirate Systems and Filter Banks*, Englewood Cliffs, NJ: Prentice Hall, 1993.
- [27] S. Mallat, *A Wavelet Tour of Signal Processing*, Academic Press, 1998.
- [28] P. P. Vaidyanathan, "Theory and design of M-channel maximally decimated quadrature mirror filters with arbitrary M, having perfect reconstruction property," *IEEE Trans. ASSP.*, pp. 476–492, Apr. 1987.
- [29] E. Lawrey, "Adaptive techniques for multiuser OFDM," *PhD dissertation, James Cook University, Australia*, 2001.
- [30] L. Hanzo, C. Wang, and M. Yee, *Adaptive wireless transceivers: turbo-coded, turbo-equalized and space-time coded TDMA, CDMA, and OFDM systems, chapter 13*, IEEE Press, 2002.
- [31] H. S. Malvar, "Lapped transforms for efficient transform/subband coding," *IEEE Transaction on Acoustics, Speech and Signal Process*, vol. 38, no. 6, June 1990.
- [32] H. S. Malvar, "Modulated QMF filter bank with perfect reconstruction," *Electronic Letters*, vol. 26, no. 13, June 1990.
- [33] R.A. Gopinath and C.S. Burrus, "On cosine-modulated wavelet orthonormal bases," *IEEE Trans. on Image Processing*, vol. 4, no. 2, pp. 162–175, Feb. 1995.
- [34] Y. Zhao and S. G. Haggman, "Ber analysis of OFDM communication systems with intercarrier interference," *in proc. ICCT'98*, vol. 2, Oct. 1998.
- [35] H. Stark and J. W. Woods, *Probability, random processes, and estimation theory for engineers*. Prentice Hall, 1994.
- [36] W. Craig, "A new, simple, and exact result for calculating the probability of error for two-dimensional signal constellations," *in Proc. IEEE Military Communication Conference, MILCOM'91*, pp. 571–575, Oct. 1991.

- [37] M. K. Simon and D. Divsalar, "Some new twists to problems involving the Gaussian probability integral," *IEEE Trans. on Communications*, vol. 46, pp. 200–210, Feb. 1998.
- [38] F. S. Weinstein, "Simplified relationships for the probability distribution of the phase of a sine wave in narrow-band normal noise," *IEEE Trans. on Information Theory*, vol. IT-20, pp. 658–661, Sept. 1974.
- [39] R. F. Pawula, S. O. Rice, and J. H. Roberts, "Distribution of the phase angle between two vectors perturbed by Gaussian noise." *IEEE Trans. on Communications*, vol. COM-30, pp. 1828–1841, Aug. 1982.
- [40] X.-P. Zhang, M. Desai, and Y.-N. Peng, "Orthogonal complex filter banks and wavelets: some properties and design," *IEEE Trans. Signal Processing*, vol. 47, no. 4, pp. 1039–1048, Apr. 1999.
- [41] H. Zou and A. H. Tewfik, "Discrete orthogonal M-band wavelet decompositions," *in proc. ICASSP*, vol. 4, pp. IV-605–608, 1992.
- [42] P. Steffen, P. N. Heller, R. A. Gopinath, and C. S. Burrus, "Theory of regular M-band wavelet bases," *IEEE Transaction on Signal Processing*, vol. 41, no. 12, Dec. 1993.
- [43] B. Manly, *Multivariate statistical methods: a primer. 2nd edition*, Chapman Hall, 1994.
- [44] S. Haykin. *Communication systems. 4th edition*. John Wiley & Sons Inc, 2001.
- [45] N. L. Johnson, S. Kotz, and N. Balakrishnan, *Discrete Multivariate Distributions*, John Wiley & Sons Inc, 1997.
- [46] H. Jeffreys and B. S. Jeffreys, *Methods of Mathematical Physics. 3rd edition.*, Cambridge University Press, Cambridge, England, 1988.